SPOROCYTELESS/NOZZLE acts together with MADS-domain transcription factors to regulate an auxin-dependent network controlling the Megaspore Mother Cell development

Alex Cavalleri[1,6], Chiara Astori[1,6], Silvia Manrique[1,3,6], Greta Bruzzaniti[1], Cezary Smaczniak[2], Chiara Mizzotti[1], Alessandro Ruiu[1], Mattia Spanò[1], Andrea Movilli[1,4], Veronica Gregis[1], Xiaocai Xu[2,5], Kerstin Kaufmann[2], Lucia Colombo[1,7]

[1]Departiment of Biosciences, University of Milan, Milano 20133, Italy.

[2] Plant Cell and Molecular Biology, Institute of Biology, Humboldt-Universität zu Berlin, Berlin 10115, Germany.

[3]Present address: Instituto de Biología Molecular y Celular de Plantas (IBMCP) (CSIC-UPV), Valencia, Spain / Departamento de Biología Vegetal, Facultad de Farmacia, Universidad de Valencia, Valencia, Spain.

[4]Present address: Department of Molecular Biology, Max Planck Institute for Biology Tübingen, 72076 Tübingen, Germany

[5]Present address: Department of physiology, Max Planck Institute for Biology Potsdam, 14476 Potsdam Brandenburg, Germany

[6]These authors contributed equally

[7]Correspondence to: lucia.colombo@unimi.it

Abstract

The formation of the female gamete is a complex developmental process that begins with the differentiation of the Megaspore Mother Cell (MMC) within the ovule.

SPOROCYTELESS/NOZZLE (SPL/NZZ) is the principal regulator of the MMC formation, as mutations in the *SPL/NZZ* gene leads to the failure of the MMC differentiation. Nonetheless, the SPL/NZZ-dependent regulatory pathway governing the MMC development remains largely unknown. Using a multi-omics approach, we identify direct SPL/NZZ targets and their downstream network. We discovered that SPL/NZZ interacts with ovule-identity MADS-domain transcription factor complexes, to regulate the expression of common target genes. By integrating the omics data with the analysis of either complementation or mutant lines, we describe a comprehensive regulatory

mechanism, in which SPL/NZZ determines the differentiation of the MMC by acting on an auxin-dependent downstream network.

Introduction

In flowering plants, sporogenesis starts with the differentiation of female and male meiocytes: Megaspore Mother Cells (MMCs) within ovules and Pollen Mother Cells (PMCs) within anthers[1,2]. In *Arabidopsis thaliana,* the master regulator of meiocytes differentiation is *SPOROCYTELESS/NOZZLE (SPL/NZZ)* since mutations in the *SPL/NZZ* gene result in a complete female and male sterility due to the absence of both the MMC and the PMC[1,2]. *SPL/NZZ* belongs to the SPEAR family which, in *A. thaliana*, consists of 5 genes[3,4]. The SPEAR proteins have a nuclear localisation signal (NLS) at the N-terminus, the SPL/NZZ motif in the middle of the protein, and an EAR motif at the C-terminus. It has been reported that, through the EAR motif, SPL/NZZ recruits co-repressors, like TOPLESS (TPL), that mediate the transcriptional repression of target genes by interacting with HDAs[3–7].

SPL/NZZ also has an additional Myc-type helix-loop-helix domain that could mediate SPL/NZZ homodimerization[2,4]. Interestingly, SPL/NZZ was initially described as a MADS-like protein, since it contains a sequence of 17 amino acids similar to the MADS-domain[2].

According to earlier reports, SPL/NZZ can interact with two families of transcription factors (TFs): the YABBY (YAB) and the CINCINNATA-like TEOSINTE BRANCHED/CYCLOIDEA/PCF (TCP). SPL interaction with these TFs mediates the transcriptional repression of their targets in plants[4,5,8].

Despite its importance for plant reproduction, the mechanisms of *SPL/NZZ* transcriptional regulation, as well as its downstream network, are still poorly understood. Among the factors involved in *SPL/NZZ* regulation, auxin signalling was shown to be a positive regulator of *SPL/NZZ* expression in anthers, as demonstrated by the reduced *SPL/NZZ* transcript accumulation in the *taa1 tar2-2* mutant[9]. AGAMOUS (AG) is one of the few factors described to regulate *SPL/NZZ* expression in both ovules and stamens. Indeed, in flowers at stages 11-13[10], AG binds a CArG-box in the *SPL/NZZ* 3' UTR to promote its expression in integuments and chalaza of the ovule. Here, *SPL/NZZ* expression pattern is also regulated by the RdDM pathway, since *SPL/NZZ* is ectopically expressed in the *drm1drm2* mutant[11].

In addition to its function in MMC and PMC differentiation, SPL/NZZ is required for ovule patterning, by negatively regulating the expression of factors such as *AINTEGUMENTA (ANT)*, *BELL1 (BEL1)*, *INNER-NO-OUTER (INO)*, and *PHABULOSA (PHB)*[12,13]. Indeed,

besides the absence of the MMC, *spl/nzz* mutant ovules are characterised by an impairment in integuments growth and a longer funiculus[12].

Concerning the SPL/NZZ downstream network, SPL/NZZ plays a crucial role in the auxin signalling pathway as the auxin-response reporter line *DR5v2* and the auxin efflux carrier *PIN-FORMED1 (PIN1)* exhibit decreased expression in the *spl/nzz* mutant ovule[14,15].

This study employs a multi-techniques approach, integrating Co-immunoprecipitation coupled with mass spectrometry (Co-IP/MS), Chromatin Immunoprecipitation and sequencing (ChIPseq), and RNA sequencing (RNAseq), to comprehensively identify direct SPL/NZZ targets and their downstream network. Our findings reveal the interaction between SPL/NZZ and ovule identity MADS-domain transcription factor complexes, thereby regulating the expression of common target genes, such as *ANT*. This activity influences the auxin signalling, which was previously suggested as a primary pathway necessary for the MMC differentiation[15]. We propose a multistep model in which MMC specification and development relies on an auxin-dependent SPL/NZZ downstream network.

Results

SPL/NZZ and MADS-domain transcription factors interact to form multimeric complexes

To gain insight into the network regulated by SPL/NZZ, essential for the specification of the MMC, we identified potential partners of SPL/NZZ during early stages of ovule development, prior to and at the MMC stage, by performing co-immunoprecipitation followed by mass spectrometry (Co-IP/MS). To do this, we took advantage of the *pSPL/NZZ::SPL/NZZ:GFP* construct, previously used to complement the strong *spl-1* mutant allele[11]. As previously described[11], at ovule stage 2-I[16], SPL/NZZ-GFP accumulated in the most apical cells of the L1 layer (Supplementary Figure 1A). From stages 2-II to stage 2-V, associated with the end of the meiosis, SPL/NZZ-GFP accumulation domain comprised the L1 layer of the whole nucellus (Supplementary Figure 1B-D). At later stages, SPL/NZZ-GFP signal decreased without changing its pattern and, at ovule maturity, SPL/NZZ-GFP was still detected in the surviving nucellar L1 cells (Supplementary Figure 1E, F).

We introduced the *pSPL/NZZ::SPL/NZZ:GFP* construct into the *pAP1::AP1:GR ap1cal* system for synchronised induction of flower development[17,18]. We performed DEX treatment on the inflorescences and evaluated the SPL/NZZ-GFP expression at different

days after induction (DAI) to select the appropriate stages for samples collection. At 3 DAI, SPL/NZZ-GFP was mainly visible in anther primordia, a result in line with SPL/NZZ activity in anther morphogenesis[2,19] (Supplementary Figure 1G-I). At 9 DAI, SPL/NZZ-GFP expression in anthers was almost absent (Supplementary Figure 1J). By contrast, despite partial loss of synchronisation at this later timepoint after AP1-GR induction, most flowers showed ovules at stage 2-I, where we could clearly observe a strong and specific nucellar SPL/NZZ-GFP accumulation (Supplementary Figure 1K-L). Therefore, we used three independent biological replicates of inflorescences at 9 DAI for Co-IP/MS, employing an anti-GFP antibody[20]. We found 660 proteins that were statistically enriched ($\log_2$ intensity difference > 0; FDR ≤ 0.05) in the IP samples with respect to the input controls. As expected, SPL/NZZ itself was found as one of the most enriched proteins (Figure 1A).

To obtain an overview regarding the function of the protein enriched in the SPL/NZZ Co-IP/MS, we performed a molecular function and biological process GO terms enrichment analysis. The most enriched categories were associated with the RNA polymerase activity, DNA binding and transcription. Moreover, we found an enrichment in biological process categories such as floral and gynoecium development, regulation of transcription and RNA processing (Figure 1B).

Since SPL/NZZ binds to the DNA by its association with transcriptional factor (TF) complexes[4,5], we focused our attention on the TFs identified among the SPL/NZZ partners. We found 56 TFs as putative SPL/NZZ interactors. Quite strikingly, among the TCPs, only TCP22 was statistically enriched in our list while none of the YABBY TFs were present. The MADS-domain TF family was the most represented in our dataset, corresponding to almost 20% of all the TFs found (Figure 1A). This list of potential MADS-domain TFs interacting with SPL/NZZ included SEEDSTICK (STK), SHATTERPROOF2 (SHP2), SEPALLATA1 (SEP1), SEPALLATA2 (SEP2), SEPALLATA3 (SEP3) and AGAMOUS (AG), all proteins previously associated to ovule specification and development[21–23].

Based on these results, we verified whether SPL/NZZ could directly interact with MADS-domain TFs in yeast. Since SPL/NZZ contains an EAR-motif, which could negatively impact on GAL4 transcriptional activation functionality, we used a SPL/NZZ variant lacking the EAR-motif sequence (SPL/NZZΔ). We initially tested the interaction between SPL/NZZΔ, fused with a GAL4 activation domain (AD) or DNA binding domain (BD) with AG, SEP3Δ[23] or STK. We found positive results for the SPL/NZZ$\Delta_{(AD)}$ - AG$_{(BD)}$, SPL/NZZ$\Delta_{(AD)}$ - STK$_{(BD)}$ and SEP3$\Delta_{(AD)}$ - SPL/NZZ$\Delta_{(BD)}$ interactions (Figure 1C, Supplementary Figure 2A). It was previously shown that the MADS-domain proteins

generate multimeric complexes to regulate target genes[22,24]. Based on this, we performed yeast-three-hybrid assays. We initially evaluated the formation of complexes using SPL/NZZΔ fused to the AD, SEP3Δ to the TFT and either STK or AG to the BD, finding positive results for the SPL/NZZ$\Delta_{(AD)}$ - SEP3$\Delta_{(TFT)}$ - STK$_{(BD)}$ and SPL/NZZ$\Delta_{(AD)}$ - SEP3$\Delta_{(TFT)}$ - AG$_{(BD)}$ interactions (Figure 1D). It is worth to notice that, even though SPL/NZZ$\Delta_{(AD)}$ did not directly interact with SEP3$\Delta_{(BD)}$ (Supplementary Figure 2A) and only modestly with STK (Figure 1C), the presence of all the three components enhanced yeast growth, suggesting the formation of a more stable complex (Figure 1D). We then tested the same interactions by fusing SPL/NZZΔ with the GAL4 BD, reconfirming the establishment of complexes with either STK and SEP3Δ or AG and SEP3Δ (Supplementary Figure 2B). Concerning the screening with SPL/NZZΔ fused with the TFT, we found that the presence of SPL/NZZ$\Delta_{(TFT)}$ did not enhance the already described SEP3-AG interaction[22] (Supplementary Figure 2C).

As we confirmed that SPL/NZZ can interact with the ovule identity MADS-domain TFs, we analysed STK, AG and SEP3 expression in the nucellus at stages 2-I, 2-II, concurrently with the MMC specification. STK and SEP3 were expressed in the nucellus, as shown by the study of GFP-fusion-protein reporter lines, with a pattern comparable to the one of SPL[25–27] (Supplementary Figure 2D-G). By contrast, AG was not expressed in the nucellus (Supplementary Figure 2H, I)[27].

It was already reported that STK-SEP3 can form a tetramer[28] while SPL/NZZ can form a homodimer[4]. Using AlphaFold3[29], we predicted *in silico* the possible formation of SEP-STK-SPL/NZZ complexes. We predicted the structure of a complex containing, respectively, two copies of SEP (1, 2, or 3), STK and SPL/NZZ. AlphaFold3 preliminary predictions could fold SPL/NZZ only from amino acid 61 to amino acid 91 forming an alpha helix, a protein portion that contains the 8 amino acids forming the SPL/NZZ-motif. Indeed, the SPL/NZZ-motif was originally predicted to be part of an alpha helix spanning from amino acids 64 to amino acid 80, which has some homology to the first helix of MADS-domain TFs[2]. For these reasons, we considered only the SPL/NZZ region spanning from amino acid 61 to 91 for further predictions. All the different simulations indicate that SPL/NZZ makes contact with the K-box of the STK-SEP tetramer (Figure 1E, F; Supplementary Figure 3).

SPL/NZZ and the MADS-domain TFs share common targets

To identify the direct targets of SPL/NZZ we used the *SPL/NZZ:GFP AP1:GR ap1cal* line to perform a ChIPseq experiment. Three biological replicates of inflorescence at 9 DAI were used for chromatin immunoprecipitation using an anti-GFP antibody[30,31]. After input and IP samples sequencing, peaks were considered significant with a fold enrichment (FE) > 0, FDR ≤ 0.05 and if present in at least 2 out of 3 biological replicates. This approach retrieved a list of 203 peaks, corresponding to 197 different genes. Around the 80% of the peaks mapped in genomic regulatory regions such as promoters, supporting the reliability of the results obtained (Figure 2A).

SPL/NZZ does not have a DNA-binding domain. This implies that SPL/NZZ binds to its direct targets *via* TF complexes in which it is recruited. To characterise which TFs mostly relate to SPL/NZZ activity, we performed a TF DNA-motif enrichment analysis. We used the MEME suite[32] to analyse the 203 peak sequences retrieved from the SPL/NZZ ChIPseq experiment. The only statistically enriched DNA binding site identified was the CArG-box consensus sequence, to which the MADS-domain TFs bind (Figure 2B)[33]. In addition, enrichment analysis against the Transcriptional Factor Target lists from both the AGRIS server[34–36] and the PlantGSAD database[37], revealed that SPL/NZZ targets were enriched in genes targeted by MADS-domain TFs as AG and SEP3 or floral homeotic factors as APETALA2 (AP2)).

If SPL/NZZ binding to the DNA depends on its association to MADS-domain TF complexes, not only SPL/NZZ and MADS-domain TFs should target the same genes, but they should bind these genes at the same genomic sequences. Based on this assumption, we determined the overlap of peaks obtained by the SPL/NZZ ChIPseq with the ones obtained from a SEP3 ChIPseq dataset[38]. The already available SEP3 ChIPseq was performed using the same induction system and tissue used for the SPL/NZZ ChIPseq, and on a similar stage of development (8 DAI). Over 90% of SPL/NZZ peaks (185 out of 203, corresponding to 182 different genes), overlapped with peaks in the SEP3 dataset, strongly supporting the cooperation between SPL/NZZ and SEP3 for binding to the DNA, at least at the developmental stages used for the ChIPseq experiments. (Figure 2C, D).

Among SPL/NZZ bound genes, we found genes previously linked to SPL/NZZ function as *ANT*[12], *YUCCA6*[39] and *PHB*[40]. Interestingly, also SPL/NZZ itself was present in the list, indicating the possible existence of a feedback loop involved in SPL/NZZ regulation.

SPL/NZZ regulates the auxin signalling network

Having identified potential direct SPL/NZZ-SEP3 target genes, we focused on their biological function to determine the mechanisms involved in the MMC differentiation. To do so, we performed a Biological Process GO terms enrichment analysis using the SPL/NZZ-SEP3 common targets (Figure 2E). Besides categories associated with reproductive organs differentiation, the most enriched terms were related to auxin metabolism and biosynthesis, suggesting a direct link between SPL/NZZ and auxin (Figure 2E; 2).

To identify the genes whose expression was modified in the absence of SPL/NZZ, and the pathways associated with SPL/NZZ activity, we performed RNA sequencing on wild type (Col-0) and *spl-1* mutant pistils at stage 9[41,42]. Differential expression analysis retrieved a list of 6877 differentially expressed genes (DEGs) (FDR ≤ 0.05) (3). The Biological Process GO term enrichment analysis on the downregulated genes revealed enrichment in terms associated with chromatin remodelling and floral development (Supplementary Figure 4A). By contrast, Biological Process GO term enrichment analysis done on the upregulated genes confirmed an impairment in auxin biosynthesis, metabolism and signalling (Supplementary Figure 4B). We also observed enrichment in categories involved in cell cycle regulation, cell wall modification and callose deposition, processes known to be required for the MMC specification[43].

Taking these data into account, we chose to focus on the study of the auxin response pathway in *spl-1* ovule primordia. Particularly, we evaluated auxin transport, accumulation and response.

In wild-type ovule primordia, auxin is produced at the chalazal pole and is polarly transported towards the primordium apex mainly by PIN1, generating a region of high signalling output at the nucellus tip[44–46]. Auxin is then directed toward the L2 layer by PIN3 and PIN1 action[45]. Even though the expression of *PIN1* was shown to be reduced in the *spl-1* mutant[14,15], we observed that PIN1-GFP accumulated similarly in wild-type and *spl-1* ovules during early developmental phases (stages 1–II) (Figure 3A, C). At stage 2-III, associated with the MMC complete differentiation, the PIN1-GFP signal was drastically reduced in the *spl-1* mutant (Figure 3D) with respect to the wild type at the same stage (Figure 3B). *pPIN3:PIN3:GFP*[45,47] signal was localised at the very tip of ovule primordia in *spl-1*, and no differences were observed compared to wild type (Supplementary Figure 5A-D).

Downregulation in *PIN1* expression could negatively impact the auxin transport toward the ovule tip, resulting in a reduced auxin accumulation. Indeed, by using the *R2D2* reporter line[48], we detected a higher accumulation of DII-VENUS in the *spl-1* nucellus with respect

to wild type, which indicates a lower auxin level in the *spl-1* mutant (Supplementary Figure5E-H; Figure 3E-H, M). In addition, similarly to what was previously shown[15], *DR5v2* reporter signal[48] was hardly detected in *spl-1* mutant ovule compared to the wild type (Figure 3I-L, N), suggesting an impaired auxin response.

Since auxin accumulation was previously suggested to be required for the MMC specification[15], we believe that *PIN1* downregulation could be the main cause of MMC absence in the *spl-1* mutant ovule.

Restoring the auxin transport is sufficient to rescue the MMC differentiation in *spl-1* ovules

Although PIN1-GFP accumulation is reduced in *spl-1* ovules, *PIN1* was not present in the list of SPL/NZZ direct targets, suggesting that SPL/NZZ regulation over *PIN1* is indirect. During ovule patterning, SPL/NZZ was shown to be required for the repression of chalazal factors such as *ANT*, *BEL1*, *INO* and *PHB* in the nucellus[12,40,49]. As mentioned above, *ANT* is a direct target of the SPL/NZZ-MADS-domain TF complex. Particularly, in both SPL/NZZ and SEP3 ChIPseq datasets, we found a peak containing 4 CArG-box sequences upstream to *ANT* TSS (Supplementary Figure 6A). Absence of SPL/NZZ function determines *ANT* ectopic expression in the nucellus[12] (Supplementary Figure 6B-I). Since it was previously described that MMC differentiation was rescued in the *spl/nzz ant* double mutant[12], we hypothesise that ANT could act as a regulator of *PIN1*, causing *PIN1* downregulation in the *spl-1* nucellus. Even though we did not found *PIN1* among ANT direct-target genes[50], we observed that *PIN1* was ectopically expressed in the chalaza and funiculus of *ant.4* mutant ovules with respect to the wild type (Supplementary Figure 6J-Q). This suggests that, in ovules, ANT acts as an indirect local repressor of *PIN1*.

Based on our present and previously reported observations[15], we hypothesised that restoring polar auxin transport in the *spl-1* ovule might be sufficient to recover the MMC differentiation. Therefore, we developed the *pSPL/NZZ::PIN1* construct and we transformed it into *spl-1* mutant plants. Four distinct *spl-1* lines expressing the *pSPL/NZZ::PIN1* construct were characterised (Supplementary Figures 7A, B).

In contrast with the *spl-1* situation (Figure 4F-J, P), in *spl-1 pSPL/NZZ::PIN1,* ovule developmental defects were almost completely restored (Figure 4A-E, K-P; Supplementary Figure 7C). The MMC was correctly specified (Figure 4C, D, M, N), and completed the megasporogenesis (Figure 4E, O). Indeed, fertile ovules were formed and fertilized by pollen produced by the same plants, showing that the *pSPL/NZZ:PIN1* had rescued also

the PMC defects (Supplementary Figure 7D). Interestingly, *spl-1 pSPL/NZZ:PIN1* ovules showed also a rescue of *spl-1* integuments defect (Figure 4G-J, L-O). Nevertheless, similarly to the *spl-1* mutant, the funiculus length in *spl-1 pSPL/NZZ::PIN1* ovules remained statistically longer with respect to the wild type (Supplementary Figure 7E, F).

The inhibition of ARFs activity phenocopy the *spl-1* mutation

The results described above demonstrate the need of SPL/NZZ to regulate the auxin accumulation in the nucellus, which is essential for MMC specification. According to the auxin response model, auxin accumulation enhances AUX/IAAs degradation, releasing the ARFs from AUX/IAAs repressing activity[51]. This leads to the regulation of the expression of the ARF target genes. Based on this model, we hypothesised that the impairment of the MMC development in the *spl-1* mutant could be due to an altered post-translational modulation of ARFs functionality. Indeed, the reduced auxin accumulation in *spl-1* could prevent the AUX/IAAs degradation, resulting in a diminished ARFs activity that could affect the MMC differentiation. Accordingly, ovules containing an AUX/IAA isoform resistant to the auxin-depended proteasomal degradation might mimic the *spl-1* phenotype. We used the *SPL/NZZ* regulatory sequences to express a non-degradable version of IAA3/SHY2[52], named *shy2.6*[53]*,* generating the *pSPL/NZZ::shy2.6* construct. Since SHY2 was reported to interact with different ARFs[54–56], we used the *shy2.6* allele as a molecular tool to inhibit ARFs function. *shy2.6* carries a mutation in the degron motif, impairing its ability to interact with the SCF/TIR1 complex at threshold auxin level[53], remaining constitutively bound to ARFs PB1 domain[53].

We introduced the *pSPL/NZZ::shy2.6* construct in wild type plants, obtaining three independent lines expressing the transgene (Supplementary Figure 8A). Even if with different percentages, in all the lines we observed an impairment in the MMC differentiation, resembling the *spl-1* phenotype (Figure 5A-M). To confirm that the observed phenotype was caused by the inhibition of ARFs activity rather than other factors, such as a disruption of the polar auxin transport, we examined the expression of *pPIN1::PIN1:GFP* in *pSPL/NZZ::shy2.6* plants. The expression of PIN1-GFP in *pSPL/NZZ:shy2.6* resembled that of the wild type, suggesting that the observed phenotype was probably caused by an impairment in ARFs activity (Supplementary Figure 8B-E).

ARFs activity is required for the MMC differentiation

Collectively, our data support a *scenario* in which the MMC differentiation is mediated by the post-translational regulation of the ARFs action. SHY2 is able to interact with all the classA ARFs, including ARF5/MP, ARF6, ARF7, ARF8 and ARF19. Concerning the repressor ARFs, SHY2 was shown to interact with ARF4 and ARF9[54–56]. According to a ovule single-cell RNA-seq dataset[57], *MP*, *ARF6*, *ARF8* and *ARF9* are the only SHY2-interacting ARFs expressed in the nucellus at stages 1-II and 2-I. For these reasons, we initially decided to study *MP*, *ARF6*, *ARF8* and *ARF9* expression in both wild type and the *spl-1* ovules. We used previously published reporter lines to study *MP*, *ARF6* and *ARF8* domains of transcription and protein accumulation[58]. Concerning *ARF9*, as no functional protein reporter lines were available, we studied its expression pattern by *in-situ* hybridisation.

In ovule primordia, the levels of both ARF6-VENUS and ARF8-VENUS were presumably controlled at the post-translational stage, supporting previously reported observations[53] (Supplementary Figure 9E-L). Although both genes were transcribed in ovules (Supplementary Figure 9E, I), ARF6 was faintly visible solely in a limited number of cells (Supplementary Figure 9F), while ARF8 was not accumulated (Supplementary Figure 9J). By contrast, the MP-VENUS protein accumulated in the nucellus, as previously shown[58,59] (Supplementary Figure 9A, B). The three ClassA ARFs exhibited comparable expression and protein accumulation in both wild-type and *spl-1* ovules (Supplementary Figure 9A-L). Concerning *ARF9,* we detected its transcript accumulation in both wild type and *spl-1* nucellus at stage 1-II (Supplementary Figure 10A, C). At stage 2-III, *ARF9* transcript was accumulated in the MMC and the outer integument of wild-type ovules (Supplementary Figure 10B). By contrast, in the *spl-1* mutant background, *ARF9* was more widely expressed in both the nucellus and the chalaza (Supplementary Figure 10D).

Given their expression patterns, MP and ARF9 were selected as ARFs potentially involved in the downstream auxin response, essential for MMC specifications. According to our hypothesis, the absence of the MMC in the *spl-1* mutant was associated with a decrease in the nucellar auxin concentration, causing the stabilisation of the AUX/IAAs and consequently the impairment of ARFs activity. We hypothesise that increase MP or ARF9 levels in the *spl-1* background could overcome the repression operated by the AUX/IAAs, restoring the MMC specification. Therefore, we generated the *pSPL/NZZ::MP* and the *pSPL/NZZ::ARF9* constructs that we introduced in the *spl-1* mutant. We obtained two independent *spl-1 pSPL/NZZ::MP* lines while we found three *spl-1 pSPL/NZZ::ARF9* independent lines (Supplementary Figure 11A, B). In *spl-1 pSPL/NZZ::MP* plants, we

observed that approximately 10% of ovules developed an MMC (Figure 6A-F, I). However, these cells did not undergo meiosis, suggesting only a partial acquisition of the MMC identity (Supplementary Figure 11C). By contrast, the majority of *spl-1 pSPL/NZZ::ARF9* ovules differentiated an MMC which could also proceed into sporogenesis (Figure 6G, H, J), indicating the direct involvement of ARF9 for the MMC differentiation and development.

Altogether, our results highlight the regulation of the ARFs action as a key step of the SPL downstream response during the MMC differentiation.

DISCUSSION

Although the mechanisms necessary to restrict the acquisition of the MMC identity to one single cell have been addressed[60], the regulatory network controlling the MMC specification is still largely unknown. Since SPL/NZZ is a major factor controlling MMC development, we initially focused on the identification of SPL/NZZ interacting partners *in planta.* Even though previous works highlighted the TCP TFs as the main SPL/NZZ partners[4,5], in our Co-IP/MS dataset, the MADS-domain TFs resulted the most abundant TF family. The differences in SPL/NZZ partners identified by the Co-IP/MS and by the previous screenings of SPL/NZZ interactors could be partially explained by our use of the *AP1:GR*/*ap1cal* inducible system. This system allowed us to find SPL/NZZ partners within a constrained development time window. Additionally, while our experiments were performed *in planta,* the previously reported interactors were identified by yeast-two-hybrid screening[4,5]. We identified only one TCP family member among SPL/NZZ partners. Taking into consideration that a limited number of SPL/NZZ target genes were also identified as TCPs targets, we suggest that complexes including SPL/NZZ and TCPs may function predominately in others developmental stages, or tissues, with respect to the ones analysed in our experiments. On the contrary, several MADS-domain transcription factors turned out to be enriched in the SPL/NZZ Co-IP/MS data. Indeed, the genomic sequences bound by SPL/NZZ-containing complexes contained the CArG-box consensus DNA sequence, typically used by MADS-domain TFs for DNA binding.

We highlighted SEP3 as a TF putatively involved in SPL/NZZ recruitment to the DNA. Indeed, over 90% of SPL/NZZ targets were shared with SEP3, and SPL/NZZ and SEP3 bound these genes at the same genomic positions. Altogether, these data strongly support a *scenario* in which SPL/NZZ is recruited to the DNA by MADS-domain TF complexes.

The MADS-domain TFs STK, AG and SEP3 were shown to be fundamental for ovule development[21–23] forming complexes that regulate ovule identity. For instance, the interaction

among STK, AG, SEP3 and BEL1 was described of pivotal importance to determine chalaza identity and to correctly differentiate the integuments[23]. Taking into consideration the present and the previously reported findings, it became evident that MADS-domain TF complexes interact either with SPL/NZZ or BEL1 to control the nucellar and chalazal development, respectively. Indeed, the role of SPL/NZZ in repressing chalaza identity genes in the nucellus such as *ANT*, *BEL1* and *PHB* was already reported[12,40]. At the same time, SPL/NZZ ectopic expression or over expression in the nucellus, was associated to the differentiation of multiple MMC-like cells[11].

Unfortunately, genetic analyses to support the requirement of MADS-domain TFs during the MMC specification are hampered by their high redundancy and their pleiotropic roles in both carpel and ovule formation. Indeed, such analyses would require the generation of high-order MADS mutants, in which flower organs are severely impaired. For instance, higher-order mutants such as *sep1 sep2 sep3* do not form flower organs[61] and *stk shp1 shp2 ag/+* develops leaves instead of ovules[21,23]. Although the role of MADS-domain TFs in MMC formation has still a certain grade of uncertainty, the proposed mechanism of SPL/NZZ actions is supported by multiple evidence.

We show that the key mechanism for the MMC specification likely relies on the post-translational regulation of ARF TFs activity, associated with the nucellar auxin accumulation.

Re-establishing the auxin transport in the *spl-1* nucellus, by expressing *PIN1* under *SPL/NZZ* promoter, was sufficient to restore the MMC differentiation and sporogenesis (Figure 7D). At the same time, the expression of the auxin-insensitive *shy2.6* mutant protein, mimicked the *spl-1* phenotype (Figure 7E). We propose that SPL/NZZ activity ensures the correct nucellar auxin level and response by indirectly regulating the expression of *PIN1* (Figure 7A).

Likely, SPL/NZZ, acting together with SEP3 or other MADS TFs, promotes *PIN1* accumulation by repressing *ANT* expression in the nucellus. According to this, *ANT* ectopic expression in the *spl/nzz* nucellus causes a downregulation of *PIN1* and, consequently, the impaired nucellar auxin accumulation (Figure 7B). Indeed, it was reported that the *ant* mutation rescues the lack of the MMC in the *spl/nzz* mutant[12], suggesting that also the nucellar auxin level is restored in the *spl/nzz ant* double mutant (Figure 7C).

Among the factors involved in *PIN1* regulation in the ovule, ARF17 was recently highlighted as a PIN1 transcriptional activator[15]. Despite this, *ARF17* is repressed in the nucellus and absence of ARF17 function in the *carf17* mutant do not impact the MMC differentiation, suggesting that ARF17 action over PIN1 is mainly at the chalaza.

It is interesting to notice that at early ovule developmental stages, before the MMC differentiation, *PIN1* expression can be observed even in the *spl-1* ovule. In contrast, *PIN1* accumulation is impaired starting from the developmental stages associated with the MMC

formation. These data indicate the dynamics of *PIN1* regulation during ovule development, which could involve several different regulatory pathways specific for each developmental process. For instance, *PIN1* was shown to be required to drive ovule primordia formation and outgrowth[62]. The fact that the *spl-1* mutation is not associated with alteration in ovule primordia set, strengthen the hypothesis that SPL/NZZ activity over *PIN1* is temporally restricted with MMC specification.

Previous works already highlighted the connection between the auxin signalling and the MMC initiation. For instance, *ARF3* and *ARF17* silencing was shown to be required to repress the formation of multiple MMC cells[15,63].

According to our findings, auxin accumulation in the nucellus may trigger the degradation of the AUX/IAAs, leading to ARFs activation to support the MMC development (Figure 7A). Indeed, we observed that inhibiting the ARFs activity in a wild-type situation, by expressing the auxin-insensitive *shy2.6* mutant protein, mimicked the *spl-1* phenotype (Figure 7E). Among the ARFs expressed in the nucellus, we highlighted MP and ARF9 as putatively involved in the MMC specification. We observed that increase MP, and especially ARF9 levels, could partially rescue the MMC specification in *spl-1* (Figure 7F). According to this, the MMC development might relies on the cooperation between more ARF types. Even though we focus on MP and ARF9, since they both interacts with SHY2, multiple ARFs could be involved in this process. Indeed, based on ovule single-cell RNA-seq data[57], beside the ARFs previously cited, other repressor *ARFs* as *ARF1*, *ARF3*, and *ARF18* are expressed in the nucellus during the MMC differentiation, although they do not interact with SHY2.

In conclusion, our data provide a regulatory mechanism (Figure 7), in which SPL/NZZ is required for the establishment of the nucellar auxin pattern, needed for the post-translational regulation of ARF TFs responsible for MMC differentiation and development. It will be of great interest to investigate the SPL/NZZ downstream network controlling PCM differentiation. Although we have not investigated this process in detail, we speculate that a similar mechanism could also control PMC specification. Although the SPL/NZZ-interacting MADS-domain partners might be different in anthers with respect to ovules, the *pSPL/NZZ::PIN1* and *pSPL/NZZ::ARF9* constructs also rescued pollen formation in the *spl-1* mutant confirming, as previously suggested[9], the importance of auxin response also for the male germline.

Acknowledgement

AC and LC were supported by MIUR PRIN2017 and PRIN2022; CA was supported by MIUR UNIMI PhD fellowship. SM was supported by postdoctoral fellowships from Fundación Alfonso Martín-Escudero (Madrid, Spain) and UNIMI. AM was supported by a predoctoral grant from UNIMI. Research in the Kaufmann lab is funded by DFG grants 512328399, 512328399, 458750707. The Kaufmann lab wishes to thank the Dresden Concept Genome Centre for support with NGS sequencing. Mass Spec was performed using a Q Exactive Plus funded by DFG (428987924). We thank Francesca Lopez for helping during the generation of some of the lines analysed. We thank Rosanna Petrella, Simona Masiero and Marta Mendes for the helpful discussion. Part of this work was performed at the Unitech NoLimits, an advance imaging facility established by the University of Milan.

Author contribution

AC, CA, SM and LC designed the research. AC, CA, GB, CS, CM, SM, AR, MS, VG, XX performed the experiments. CA, CS, AC, GB, CM, LC and KK analysed the data. AC, CA, LC, GB, CS, SM wrote the manuscript. LC and KK supported the research

Competing interest

Authors declare no competing interests

Data availability statement

All materials reported in this study are available from the corresponding author upon request. Co-IP/MS raw data can be found under the accession XXX. CHIPseq raw data can be found under the accession XXX. RNAseq raw data can be found under the accession XXX.

Supplementary information

Supplementary Figure 1: *pSPL/NZZ::SPL/NZZ:GFP* expression

Supplementary Figure 2: Results of yeast-two- and three-hybrid assays and SEP3, STK and AG accumulation patterns in the ovule

Supplementary Figure 3: AplhaFold3 predictions of SPL/NZZ-SEPs-STK complexes

Supplementary Figure 4: Biological processes GO terms enrichment analysis of DE genes in the *spl-1* pistil with respect to the wild type

Supplementary Figure 5: *pPIN3::PIN3:GFP* expression in wild type and *spl-1* ovules and *R2D2* signal in wild type and *spl-1* ovules at stage 1-II

Supplementary Figure 6: SPL/NZZ and SEP3 ChIPseq peaks on *ANT* promoter, *ANT* expression in wild type and *spl-1* ovules and *PIN1* expression in wild type and *ant.4* ovules

Supplementary Figure 7: *pSPL/NZZ::PIN1* expression and phenotypes of the *spl-1 pSPL/NZZ::PIN1* plants

Supplementary Figure 8: *pSPL/NZZ::shy2.6* expression level and PIN1-GFP accumulation in *pSPL/NZZ::shy2.6*

Supplementary Figure 9. ClassA ARFs expression in wild type and *spl-1* ovules

Supplementary Figure 10. ARF9 expression in wild type and *spl-1* ovules detected by *in-situ* hybridisation

Supplementary Figure 11. *pSPL/NZZ::MP* and *pSPL/NZZ::ARF9* expression, *spl-1 pSPL/NZZ::MP* and *spl-1 pSPL/NZZ::ARF9* ovules at stage 2-IV

Material and methods

Plant material and growing condition

Arabidopsis thaliana Columbia-0 plants were grown in controlled condition under a long-day photoperiod (16h light 150 µm.m^{-2}.s^{-1} / 8h dark) at 22°C. *spl-1* mutant in the Col-0 background was previously described[14]. The *pSPL/NZZ::SPL/NZZ:GFP* line was previously described[11]. The *AP1:GR/ap1cal* inducible system was described in[17]. *ant.4* mutant in the Ler background was previously described[64,65]. *pSTK:STK:GFP*, *pSEP3::SEP3:GFP, pAG::AG:GFP* were previously described[25–27]. The *spl-1 pPIN1::PIN1:GFP* line was described in[14]. *pPIN3::PIN3:GFP*[66], *DR5v2*[48] and *R2D2*[48] lines were manually crossed with *spl-1* heterozygous plants.

Generation of transgenic lines

To obtain the *pSPL/NZZ::SPL/NZZ:GFP pAP1::AP1:GR ap1cal* inducible line, *pAP1::AP1:GR ap1cal* plants[17] were transformed with the *pSPL/NZZ::SPL/NZZ:GFP* construct *via* floral dip technique.

SPL/NZZ:GFP AP1:GR ap1cal plants were induced with dexamethasone treatment directly on the inflorescence-like meristem for 9 days. After the third and the ninth dexamethasone treatment, the expression of SPL/NZZ-GFP was controlled at confocal microscope.

The *pSPL/NZZ::PIN1*, *pSPL/NZZ::shy2.6*, *pSPL/NZZ::MP* and *pSPL/NZZ::ARF9* constructs were obtained with the multisite gateway cloning technique. *PIN1*, *shy2.6*, *MP* and *ARF9* CDS sequences were amplified using the Q5 High-Fidelity DNA polymerase (NEB) and cloned into the *pDONR221* plasmid, according to the BP II protocol (Invitrogen, cat. number: 11789020). Multi-site LR reactions were performed using the *pDONR221 P1-P4* containing the *SPL/NZZ* promoter sequence[11]; the p*DONR221* containing either *PIN1*, *shy2.6*, *MP* or *ARF9*; the *pDONR221 P3-P2* carrying the *SPL/NZZ 3'UTR* sequence[11] and the destination vector *pH7m34GW*[67], according to the LR II Plus protocol (Invitrogen, cat. number: 12538120). Thanks to the floral dip technique, *pSPL/NZZ::PIN1, pSPL/NZZ::MP* and *pSPL/NZZ::ARF9* were transformed into the *SPL/NZZ / spl-1* heterozygous background, whereas *pSPL/NZZ::shy2.6* was transformed into wild-type Col-0 plants.

RT-qPCR expression analysis

For each sample, 5 inflorescences pooled together (comprising flowers spanning from stage 1 to stage 12), were used for total RNA extraction. RNA extraction was performed using the Macherey-Nagel NucleoSpin RNA plus kit (Item number: 740984.50) according to the manual instructions. 500 ng of DNA-clean total RNA for each sample were retrotranscribed using the Bio-Rad iScript™ Reverse Transcription Supermix for RT-qPCR (Bio-Rad, cat number: 1708840). cDNA was used for RT-qPCR using the Bio-Rad iTaq Universal SYBR Green Supermix (Bio-Rad, cat number: 1725120). *ACTIN8* was used as housekeeping normaliser for relative normalised expression calculation. Expression levels were expressed as mean ± SEM among three technical replicated.

Analysis of ovules morphology by confocal and optical microscopy

Ovules morphology was evaluated by both confocal and optical widefield microscopy. For confocal microscopy, pistils were manually dissected from the flowers and mounted in a solution of 10 µg/ml Renaissance2200 (Renaissance Chemicals, SR2200). Samples were immediately imaged using a Nikon AX confocal microscope. Renaissance2200 was exited

at 405 nm and emission signal was detected between 440-470 nm. For widefield microscopy, inflorescences were collected in a solution 9:1 ethanol/acetic acid. After 24 hours at 4°C, inflorescences were transferred to a solution 70% ethanol. Pistils were manually dissected and mounted in chloral hydrate clearing solution before microscopic imaging. Analysis of percentage of ovules developing the MCC in wild type, *spl-1, spl-1 pSPL/NZZ::PIN1*, *pSPL/NZZ::shy2.6*, *spl-1 pSPL/NZZ:MP* and *spl-1 pSPL/NZZ:ARF9* was performed on ovules at stages 2-II, 2-III.

For fluorescent reporter lines signals imaging, pistils were mounted in the Renaissance2200 solution and imaged using a Nikon AX confocal microscope. mTQ was exited with a 445nm laser and detected at 480-490nm. GFP was excited with a 488 nm laser and detected at 520-540 nm. VENUS was excited with a 514 nm laser and detected at 530-560nm. tdTOMATO was exited with a 514 nm laser and detected at 570-630 nm. Imaging was performed with sequential settings to eliminate signal crosstalk. Confocal images were analysed with the Fiji software[68]. For the *DR5v2* signal quantification, the Renaissance2200 channel, showing the cellular organisation, has been used to define a region of interest (ROI) comprising the whole ovule nucellus. The mean tdTOMATO signal has been subsequentially measured in the ROI. The *R2D2* signal was analysed as previously described[58]. The tdTOMATO channel has been used to generate a binary mask indicating the nucellar nucelli showing *R2D2* expression. The VENUS and the tdTOMATO mean signals in the single nuclei were subsequentially measured.

Co-IP/MS material generation and data analysis

IP-MS experiments were performed as described before[20]. Essentially, nuclei were isolated from the unfixed plant tissues. Proteins, including native protein complexes, were extracted from nuclei extracts and immunoprecipitated with the GFP antibody using µMACS GFP Isolation Kit (Miltenyi Biotec, cat. number: 130-091-288). Immunoprecipitated proteins were released from the beads with 8 M urea. As control, protein extracts from before the immunoprecipitation were used and processed with the FAST method[69]. Eluted proteins were reduced with DTT, alkylated with IAA and digested with Trypsin/Lys-C Mix, Mass Spec Grade (Promega, cat. number: V5071). Resulting peptides were desalted, dried and resuspended in a loading solution. Peptide concentration was estimated using NanoDrop One A205 method. Samples were analyzed using the EASY-nLC 1200 (Thermo

Fisher Scientific™) coupled to the Q Exactive Plus mass spectrometer (Thermo Fisher Scientific™). Peptides were loaded onto the Acclaim PepMap 100 C18 analytical column and separated with a linear solvent B gradient of 5% to 40 % over 70 min and 40% to 50% over 5 min. Tandem MS spectra (MS/MS) were acquired in the data-dependent acquisition (DDA) mode using a TOP15 approach.

The RAW peptide sequencing data obtained from the Q Exactive Plus were processed by the MaxQuant (version 1.6.14.0) software. Settings of the MaxQuant were mostly kept default with “label-free quantification (LFQ)”, “iBAQ” and “Match between runs” options on. The protein database was *Arabidopsis thaliana* UniProt UP000006548 without protein isoforms. After the MaxQuant analysis, the output proteinGroups.txt file was taken for further filtering and statistical analysis in the Perseus (version 1.6.15.0) software. The protein LFQ intensity data was $\log_2$-transformed. Proteins identified by only modified peptides (“Only identified by site”), by reverse sequence database (“Reverse”) and protein contaminants (“Potential Contaminant”) were removed from the analysis. Proteins with LFQ intensity values in at least two biological replicates and proteins with at least two unique peptides were kept. Missing protein LFQ intensity values were replaced only in the input samples by the imputation from the left arm of the LFQ intensity normal distribution (0.3 width, 1.8 down shift, separately for each column) to emulate background protein level. Relative protein amount differences were evaluated by two-sample t-tests with permutation-based FDR correction and S0 parameter set to 1.0. The GO term enrichment analyses were performed with clusterProfiler[70], with default parameters. The statistical significance of enriched categories was determined by the Benjamini-Hochberg (FDR) test[71], considering significant only categories with FDR ≤ 0.05. GO term enrichment analyses were performed on R studio, version 4.4.1.

ChIPseq material generation and data analysis

ChIPseq experiments were performed as described before[30,31]. Specifically, plant tissues were fixed in 1% formaldehyde solution, frozen in liquid nitrogen and ground to a fine powder. Nuclei were isolated through a sequential wash with buffer containing 0.5% Triton X-100 and lysed followed by chromatin sheering by sonication. After chromatin clearing, immunoprecipitation was performed with the GFP antibody (Abcam, ab290) followed by incubation with protein A magnetic beads (Thermo Fisher Scientific™, cat. number: 88845). The immunoprecipitated chromatin was released from the beads and de-crosslinked. The input sample, corresponding to the protein extract from before the

immunoprecipitation, was also de-crosslinked and used as a ChIP control. The DNA was purified and concentrated using DNA Clean & Concentrator-5 kit (Zymo Research, cat. number: D4004) following manufacturer's instructions and eluted with 20 µl of the DNA Elution Buffer. The DNA sequencing libraries for both ChIP and Input samples were prepared using ThruPLEX DNA-Seq Kit (Takara Bio, cat. number: R400674) and SMARTer DNA Unique Dual Index Kit (Takara Bio, cat. number: R400697) following manufacturer's instructions. DNA double size selection 100-700 bp was performed using SPRIselect beads (Beckman Coulter, cat. number: B23317). DNA libraries were sequenced on the Illumina sequencer.

Raw data were trimmed using Trimmomatic 0.39[72] with the following parameters: ILLUMINACLIP :1:30:6, LEADING: 3, TRAILING: 3, HEADCROP: 10, AVGQUAL: 20, MINLEN: 35. Mapping was performed using Bowtie 2[73] on TAIR10 genome. Duplicated reads were removed using SAMtools[74]. The peak calling was performed with MACS2[75] with -g 118459858. Peaks enrichment statistical significance was evaluated according to the Benjamini-Hochberg (FDR) test. Peaks were merged using BEDTools[76]. Only peaks present in at least 2 out of 3 biological replicates were considered. Peaks annotation was performed with ChIPseeker[77] with the following parameters: tssRegion comprised between -3000 and 0 and the genomicAnnotationPriority to 5UTR, 3UTR, Exon, Intron, Promoter, Downstream and Intergenic. The GO term enrichment analysis was performed with clusterProfiler[70], with default parameters. The statistical significance of enriched categories was determined by the Benjamini-Hochberg (FDR) test, considering significant only categories with FDR ≤ 0.05. Peak annotation and the GO term enrichment analysis were performed on R studio, version 4.4.1. The consensus sequence enrichment analysis was performed using the MEME suite [32] with default parameters. The analysis of common peaks between the SPL/NZZ ChIPseq and the SEP3 ChIPseq has been performed by using the command subsetByOverlaps on R studio, version 4.4.1.

In-silico prediction of protein complex structures

Protein complex structure predictions were performed with the AlphaFold3 tool with default parameters. Protein sequences and domains annotation of SPL/NZZ (AT4G27330), STK (AT4G09960), SEP1 (AT5G15800), SEP2 (AT3G02310) and SEP3 (AT1G24260), were retrieved from the Uniprot database. AlphaFold3 models were analysed with the PyMOL software.

RNAseq material generation and data analysis

Three biological replicates of wild-type and *spl-1* pistils at stage 9[42] were collected in the NucleoProtect RNA (Macherey-Nagel, cat. number: 740750.500) and stored at 4°C for one day. RNA extraction was performed using the NucleoSpin RNA kit (Macherey-Nagel).

RNA was sequenced with the Novaseq X, at a depth of 30M reads with a paired-end sequencing.

Raw data were trimmed using Trimmomatic 0.39[72] with the following parameters: ILLUMINACLIP :1:30:6, LEADING: 3, TRAILING: 3, HEADCROP: 10, AVGQUAL: 20, MINLEN: 35. Mapping was performed with STAR[78], with --alignIntronMax 10000 on TAIR10 genome. Counts were obtained with featureCounts[79], using TAIR11 annotation.

Counts were filtered with HTSFilter[80] and the DEGs were obtained using DESeq2[81], considering statistically differentially expressed DEGs with an FDR ≤ 0.05, as determined by the Benjamini-Hochberg (FDR) test. The GO terms enrichment analyses were performed with clusterProfiler[70]. Only categories with an FDR ≤ 0.05, according to the Benjamini-Hochberg (FDR) test were considered statistically significant. DEGs evaluation and GO terms enrichment analyses were performed on R studio, version 4.4.1.

***In-situ* hybridisation**

In-situ hybridizations were performed as indicated in[62]. Developing inflorescences were fixed in Formaldehyde/Ethanol/Acetic Acid (3.7%/50%/5%) and embedded in paraffin. Fixed and embedded tissues were sectioned to 8 µm thickness with microtome. *PIN1*, *ANT* and *ARF9* anti-sense probes were obtained from retrotranscribed RNA extracted from wild-type inflorescences.

Yeast-two- and three-hybrid assays

Yeast-two- and three-hybrid assays were performed following the protocol from[82] with some modifications.

Both yeast-two- and three-hybrid assays were performed at 28°C using a single AH109 yeast strain *via* co-transformation, or AH109 and Y187 yeast strains through co-transformation and mating.

The interactions were tested in selective media lacking leucine, tryptophan, histidine and adenine. AG and STK full-length CDS and SPL/NZZ and SEP3Δ shorter versions (SPL/NZZΔ and SEP3Δ respectively) were cloned into Gateway vector GAL4 system (pGBKT7 and pGADT7, Clontech; pTFT1[83]).

Statistical information

The SPL/NZZ Co-IP/MS experiment has been performed on three independent biological replicates of *pSPL/NZZ::SPL/NZZ:GFP pAP1::AP1:GR ap1cal* inflorescences at 9 DAI. Proteins with LFQ intensity values in 2 out of 3 biological replicates and with at least two unique peptides were kept. Relative protein amount differences were evaluated by two-sample t-tests with permutation-based FDR correction and S0 parameter set to 1.0.

The SPL/NZZ ChIPseq experiment has been performed on three independent biological replicates of *pSPL/NZZ::SPL/NZZ:GFP pAP1::AP1:GR ap1cal* inflorescences at 9 DAI. Peaks with an FDR ≤ 0.05 and present in at least 2 out of 3 biological replicates were considered. Statistical significance was evaluated according to the Benjamini-Hochberg (FDR) test.

Statistical significance of SPL/NZZ target genes enrichment against AGRIS and PlantGSAD transcriptional factor target lists has been evaluated with the ShinyGo[84] webtool, and only categories with an FDR ≤ 0.05 were considered significant.

The *spl-1* vs wild type RNAseq experiment has been performed on three independent biological replicates of wild type and *spl-1* pistils at stage 9 of development. Statistical significance of *spl-1* vs wild-type DEGs was evaluated with the Benjamini-Hochberg (FDR) test and only genes with an FDR ≤ 0.05 were considered significant.

Statistical significance of Gene Ontology enrichment analyses on the results obtained from the SPL/NZZ Co-IP/MS, the SPL/NZZ ChIPseq and the *spl-1* vs wild type RNAseq, was evaluated according to the Benjamini-Hochberg (FDR) test. Categories with an FDR ≤ 0.05 were considered significant.

For the *R2D2* and *DR5v2* signal intensity measurements, statistical significance has been evaluated according to the results the student's t-test, two-tailed distribution homoscedastic, confronting the mutant with the wild-type. Comparisons with a $p \leq 0.05$ were considered significant. student's t-test calculation has been performed with Microsoft Excell. For the morphological analyses of ovules differentiating an MMC, as well as funiculus length measurements, statistical significance has been evaluated according to the results of one-way ANOVA with post-hoc Tukey HSD test. Comparisons with a $p \leq 0.05$ were considered significant. The analysis has been performed with the webtool: https://astatsa.com/OneWay_Anova_with_TukeyHSD/.

References

1. Schiefthaler, U. *et al.* Molecular analysis of NOZZLE, a gene involved in pattern formation and early sporogenesis during sex organ development in Arabidopsis thaliana. *Proc. Natl. Acad. Sci. U. S. A.* **96**, 11664–11669 (1999).
2. Yang, W. C., Ye, D., Xu, J. & Sundaresan, V. The SPOROCYTELESS gene of Arabidopsis is required for initiation of sporogenesis and encodes a novel nuclear protein. *Genes Dev.* **13**, 2108–2117 (1999).
3. Tao, Q. *et al.* The TIE1 transcriptional repressor links TCP transcription factors with TOPLESS/TOPLESS-RELATED corepressors and modulates leaf development in Arabidopsis. *Plant Cell* **25**, 421–437 (2013).
4. Chen, G.-H., Sun, J.-Y., Liu, M., Liu, J. & Yang, W.-C. SPOROCYTELESS Is a Novel Embryophyte-Specific Transcription Repressor that Interacts with TPL and TCP Proteins in Arabidopsis. *J. Genet. Genomics* **41**, 617–625 (2014).
5. Wei, B. *et al.* The molecular mechanism of SPOROCYTELESS/NOZZLE in controlling Arabidopsis ovule development. *Cell Res.* **25**, 121–134 (2015).
6. Szemenyei, H., Hannon, M. & Long, J. A. TOPLESS mediates auxin-dependent transcriptional repression during Arabidopsis embryogenesis. *Science (80-.).* **319**, 1384–1386 (2008).
7. Wang, L., Kim, J. & Somers, D. E. Transcriptional corepressor TOPLESS complexes with pseudoresponse regulator proteins and histone deacetylases to regulate circadian transcription. *Proc. Natl. Acad. Sci. U. S. A.* **110**, 761–766 (2013).
8. Sieber, P., Petrascheck, M., Barberis, A. & Schneitz, K. Organ polarity in Arabidopsis. NOZZLE physically interacts with members of the YABBY family. *Plant Physiol.* **135**, 2172–2185 (2004).
9. Zheng, Y. *et al.* Auxin guides germ-cell specification in Arabidopsis anthers. *Proc. Natl. Acad. Sci. U. S. A.* **118**, (2021).
10. Ito, T. *et al.* The homeotic protein AGAMOUS controls microsporogenesis by regulation of SPOROCYTELESS. *Nature* **430**, 356–360 (2004).
11. Mendes, M. A. *et al.* The RNA-dependent DNA methylation pathway is required to restrict SPOROCYTELESS/NOZZLE expression to specify a single female germ cell precursor in Arabidopsis. *Development* **147**, (2020).
12. Balasubramanian, S. & Schneitz, K. NOZZLE regulates proximal-distal pattern formation, cell proliferation and early sporogenesis during ovule development in Arabidopsis thaliana. *Development* **127**, 4227–4238 (2000).
13. Schneitz, K., Baker, S. C., Gasser, C. S. & Redweik, A. Pattern formation and

growth during floral organogenesis: HUELLENLOS and AINTEGUMENTA are required for the formation of the proximal region of the ovule primordium in Arabidopsis thaliana. *Development* **125**, 2555–2563 (1998).

14. Bencivenga, S., Simonini, S., Benková, E. & Colombo, L. The transcription factors BEL1 and SPL are required for cytokinin and auxin signaling during ovule development in Arabidopsis. *Plant Cell* **24**, 2886–2897 (2012).
15. Huang, J. *et al.* Specification of female germline by microRNA orchestrated auxin signaling in Arabidopsis. *Nat. Commun.* **13**, 1–14 (2022).
16. Vijayan, A. *et al.* A digital 3D reference atlas reveals cellular growth patterns shaping the arabidopsis ovule. *Elife* **10**, 1–38 (2021).
17. O'Maoiléidigh, D. S. & Wellmer, F. A floral induction system for the study of early Arabidopsis flower development. *Methods Mol. Biol.* **1110**, 307–314 (2014).
18. Ó'Maoiléidigh, D. S. *et al.* Control of reproductive floral organ identity specification in arabidopsis by the C function regulator AGAMOUS. *Plant Cell* **25**, 2482–2503 (2013).
19. Zhao, F. *et al.* Phosphorylation of SPOROCYTELESS/NOZZLE by the MPK3/6 Kinase Is Required for Anther Development. *Plant Physiol.* **173**, 2265–2277 (2017).
20. Smaczniak, C. Immunoprecipitation-Mass Spectrometry (IP-MS) of Protein-Protein Interactions of Nuclear-Localized Plant Proteins. *Methods Mol. Biol.* **2698**, 163–181 (2023).
21. Pinyopich, A. *et al.* Assessing the redundancy of MADS-box genes during carpel and ovule development. *Nature* **424**, 85–88 (2003).
22. Favaro, R. *et al.* MADS-box protein complexes control carpel and ovule development in Arabidopsis. *Plant Cell* **15**, 2603–2611 (2003).
23. Brambilla, V. *et al.* Genetic and molecular interactions between BELL1 and MADS box factors support ovule development in Arabidopsis. *Plant Cell* **19**, 2544–2556 (2007).
24. Espinosa-Soto, C., Immink, R. G. H., Angenent, G. C., Alvarez-Buylla, E. R. & de Folter, S. Tetramer formation in Arabidopsis MADS domain proteins: analysis of a protein-protein interaction network. *BMC Syst. Biol.* **8**, 9 (2014).
25. Mizzotti, C. *et al.* SEEDSTICK is a master regulator of development and metabolism in the Arabidopsis seed coat. *PLoS Genet.* **10**, e1004856 (2014).
26. Smaczniak, C. *et al.* Characterization of MADS-domain transcription factor complexes in Arabidopsis flower development. *Proc. Natl. Acad. Sci. U. S. A.* **109**,

1560–1565 (2012).

27. Urbanus, S. L. *et al.* In planta localisation patterns of MADS domain proteins during floral development in Arabidopsis thaliana. *BMC Plant Biol.* **9**, 1–16 (2009).

28. Mendes, M. A. *et al.* MADS Domain Transcription Factors Mediate Short-Range DNA Looping That Is Essential for Target Gene Expression in Arabidopsis . *Plant Cell* **25**, 2560–2572 (2013).

29. Abramson, J. *et al.* Accurate structure prediction of biomolecular interactions with AlphaFold 3. *Nature* **630**, 493–500 (2024).

30. van Mourik, H., Muiño, J. M., Pajoro, A., Angenent, G. C. & Kaufmann, K. Characterization of in vivo DNA-binding events of plant transcription factors by ChIP-seq: experimental protocol and computational analysis. *Methods Mol. Biol.* **1284**, 93–121 (2015).

31. Kaufmann, K. *et al.* Chromatin immunoprecipitation (ChIP) of plant transcription factors followed by sequencing (ChIP-SEQ) or hybridization to whole genome arrays (ChIP-CHIP). *Nat. Protoc.* **5**, 457–472 (2010).

32. Bailey, T. L. *et al.* MEME SUITE: tools for motif discovery and searching. *Nucleic Acids Res.* **37**, W202-8 (2009).

33. Folter, S. de & Angenent, G. C. trans meets cis in MADS science. *Trends Plant Sci.* **11**, 224–231 (2006).

34. Yilmaz, A. *et al.* AGRIS: the Arabidopsis Gene Regulatory Information Server, an update. *Nucleic Acids Res.* **39**, D1118–D1122 (2011).

35. Palaniswamy, S. K. *et al.* AGRIS and AtRegNet. a platform to link cis-regulatory elements and transcription factors into regulatory networks. *Plant Physiol.* **140**, 818–829 (2006).

36. Davuluri, R. V *et al.* AGRIS: Arabidopsis Gene Regulatory Information Server, an information resource of Arabidopsis cis-regulatory elements and transcription factors. *BMC Bioinformatics* **4**, 25 (2003).

37. Ma, X. *et al.* PlantGSAD: a comprehensive gene set annotation database for plant species. *Nucleic Acids Res.* **50**, D1456–D1467 (2022).

38. Pajoro, A. *et al.* Dynamics of chromatin accessibility and gene regulation by MADS-domain transcription factors in flower development. *Genome Biol.* **15**, R41 (2014).

39. Li, L.-C. *et al.* SPOROCYTELESS modulates YUCCA expression to regulate the development of lateral organs in Arabidopsis. *New Phytol.* **179**, 751–764 (2008).

40. Sieber, P. *et al.* Pattern formation during early ovule development in Arabidopsis

thaliana. *Dev. Biol.* **273**, 321–334 (2004).

41. Manrique, S. *et al.* HISTONE DEACETYLASE19 Controls Ovule Number Determination and Transmitting Tract Differentiation. *Plant Physiol.* **194**, 2117–2135 (2024).

42. Smyth, D. R., Bowman, J. L. & Meyerowitz, E. M. Early flower development in Arabidopsis. *Plant Cell* **2**, 755–767 (1990).

43. Pinto, S. C. *et al.* Germline β-1,3-glucan deposits are required for female gametogenesis in Arabidopsis thaliana. *Nat. Commun.* **15**, 5875 (2024).

44. Benková, E. *et al.* Local, Efflux-Dependent Auxin Gradients as a Common Module for Plant Organ Formation. *Cell* **115**, 591–602 (2003).

45. Ceccato, L. *et al.* Maternal Control of PIN1 Is Required for Female Gametophyte Development in Arabidopsis. *PLoS One* **8**, 2–8 (2013).

46. Robert, H. S., Crhak Khaitova, L., Mroue, S. & Benková, E. The importance of localized auxin production for morphogenesis of reproductive organs and embryos in Arabidopsis. *J. Exp. Bot.* **66**, 5029–5042 (2015).

47. Žádníkova, P. *et al.* Role of PIN-mediated auxin efflux in apical hook development of Arabidopsis thaliana. *Development* **137**, 607–617 (2010).

48. Liao, C. Y. *et al.* Reporters for sensitive and quantitative measurement of auxin response. *Nat. Methods* **12**, 207–210 (2015).

49. Balasubramanian, S. & Schneitz, K. NOZZLE links proximal-distal and adaxial-abaxial pattern formation during ovule development in Arabidopsis thaliana. *Development* **129**, 4291–4300 (2002).

50. Krizek, B. A., Blakley, I. C., Ho, Y.-Y., Freese, N. & Loraine, A. E. The Arabidopsis transcription factor AINTEGUMENTA orchestrates patterning genes and auxin signaling in the establishment of floral growth and form. *Plant J.* **103**, 752–768 (2020).

51. Weijers, D. & Wagner, D. Transcriptional Responses to the Auxin Hormone. *Annu. Rev. Plant Biol.* **67**, 539–574 (2016).

52. Tian, Q., Uhlir, N. J. & Reed, J. W. Arabidopsis SHY2/IAA3 Inhibits Auxin-Regulated Gene Expression. *Plant Cell* **14**, 301–319 (2002).

53. Knox, K., Grierson, C. S. & Leyser, O. AXR3 and SHY2 interact to regulate root hair development. *Development* **130**, 5769–5777 (2003).

54. Piya, S., Shrestha, S. K., Binder, B., Neal Stewart, C. & Hewezi, T. Protein-protein interaction and gene co-expression maps of ARFs and Aux/IAAs in Arabidopsis.

Front. Plant Sci. **5**, 1–9 (2014).

55. Vernoux, T. *et al.* The auxin signalling network translates dynamic input into robust patterning at the shoot apex. *Mol. Syst. Biol.* **7**, (2011).

56. Wanamaker, S. A. *et al.* CrY2H-seq: a massively multiplexed assay for deep-coverage interactome mapping. *Nat. Methods* **14**, 819–825 (2017).

57. Hou, Z. *et al.* High-throughput single-cell transcriptomics reveals the female germline differentiation trajectory in Arabidopsis thaliana. *Commun. Biol.* **4**, 1149 (2021).

58. Cavalleri, A. *et al.* Auxin-dependent post-translational regulation of MONOPTEROS in the Arabidopsis root. *Cell Rep.* **43**, 115083 (2024).

59. Cucinotta, M. *et al.* Alternative Splicing Generates a MONOPTEROS Isoform Required for Ovule Development. *Curr. Biol.* **31**, 892-899.e3 (2021).

60. Pinto, S. C., Mendes, M. A., Coimbra, S. & Tucker, M. R. Revisiting the Female Germline and Its Expanding Toolbox. *Trends Plant Sci.* **24**, 455–467 (2019).

61. Pelaz, S., Ditta, G. S., Baumann, E., Wisman, E. & Yanofsky, M. F. B and C floral organ identity functions require SEPALLATA MADS-box genes. *Nature* **405**, 200–203 (2000).

62. Galbiati, F. *et al.* An integrative model of the control of ovule primordia formation. *Plant J.* **76**, 446–455 (2013).

63. Su, Z. *et al.* The THO Complex Non-Cell-Autonomously Represses Female Germline Specification through the TAS3-ARF3 Module. *Curr. Biol.* **27**, 1597-1609.e2 (2017).

64. Losa, A., Colombo, M., Brambilla, V. & Colombo, L. Genetic interaction between AINTEGUMENTA (ANT) and the ovule identity genes SEEDSTICK (STK), SHATTERPROOF1 (SHP1) and SHATTERPROOF2 (SHP2). *Sex. Plant Reprod.* **23**, 115–121 (2010).

65. Baker, S. C., Robinson-Beers, K., Villanueva, J. M., Gaiser, J. C. & Gasser, C. S. Interactions among genes regulating ovule development in Arabidopsis thaliana. *Genetics* **145**, 1109–1124 (1997).

66. Zádníková, P. *et al.* Role of PIN-mediated auxin efflux in apical hook development of Arabidopsis thaliana. *Development* **137**, 607–617 (2010).

67. Karimi, M., De Meyer, B. & Hilson, P. Modular cloning in plant cells. *Trends Plant Sci.* **10**, 103–105 (2005).

68. Schindelin, J. *et al.* Fiji: An open-source platform for biological-image analysis. *Nat. Methods* **9**, 676–682 (2012).

69. Wiśniewski, J. R., Zougman, A., Nagaraj, N. & Mann, M. Universal sample preparation method for proteome analysis. *Nat. Methods* **6**, 359–362 (2009).
70. Yu, G., Wang, L.-G., Han, Y. & He, Q.-Y. clusterProfiler: an R package for comparing biological themes among gene clusters. *OMICS* **16**, 284–287 (2012).
71. Benjamini, Y., Hochberg, Y. & Benjamini, Yoav, H. Y. Benjamini and Y FDR.pdf. *Journal of the Royal Statistical Society. Series B (Methodological)* vol. 57 289–300 at http://www.stat.purdue.edu/~doerge/BIOINFORM.D/FALL06/Benjamini and Y FDR.pdf%5Cnhttp://engr.case.edu/ray_soumya/mlrg/controlling_fdr_benjamini95.pdf (1995).
72. Bolger, A. M., Lohse, M. & Usadel, B. Trimmomatic: A flexible trimmer for Illumina sequence data. *Bioinformatics* **30**, 2114–2120 (2014).
73. Langmead, B. & Salzberg, S. L. Fast gapped-read alignment with Bowtie 2. *Nat. Methods* **9**, 357–359 (2012).
74. Li, H. *et al.* The Sequence Alignment/Map format and SAMtools. *Bioinformatics* **25**, 2078–2079 (2009).
75. Zhang, Y. *et al.* Model-based Analysis of ChIP-Seq (MACS). *Genome Biol.* **9**, R137 (2008).
76. Quinlan, A. R. & Hall, I. M. BEDTools: a flexible suite of utilities for comparing genomic features. *Bioinformatics* **26**, 841–842 (2010).
77. Yu, G., Wang, L.-G. & He, Q.-Y. ChIPseeker: an R/Bioconductor package for ChIP peak annotation, comparison and visualization. *Bioinformatics* **31**, 2382–2383 (2015).
78. Dobin, A. *et al.* STAR: ultrafast universal RNA-seq aligner. *Bioinformatics* **29**, 15–21 (2013).
79. Liao, Y., Smyth, G. K. & Shi, W. featureCounts: an efficient general purpose program for assigning sequence reads to genomic features. *Bioinformatics* **30**, 923–930 (2014).
80. Rau, A., Gallopin, M., Celeux, G. & Jaffrézic, F. Data-based filtering for replicated high-throughput transcriptome sequencing experiments. *Bioinformatics* **29**, 2146–2152 (2013).
81. Love, M. I., Huber, W. & Anders, S. Moderated estimation of fold change and dispersion for RNA-seq data with DESeq2. *Genome Biol.* **15**, 1–21 (2014).
82. Gietz, D., Jean, A. S., Woods, R. A. & Schiestl, R. H. Improved method for high efficiency transformation of intact yeast cells. *Nucleic Acids Res.* **20**, 1425 (1992).

83. Gutierrez-Cortines, M. E. & Davies, B. Beyond the ABCS: Ternary complex formation in the control of floral organ identity. *Trends Plant Sci.* **5**, 471–476 (2000).

84. Ge, S. X., Jung, D., Jung, D. & Yao, R. ShinyGO: A graphical gene-set enrichment tool for animals and plants. *Bioinformatics* **36**, 2628–2629 (2020).

Figures

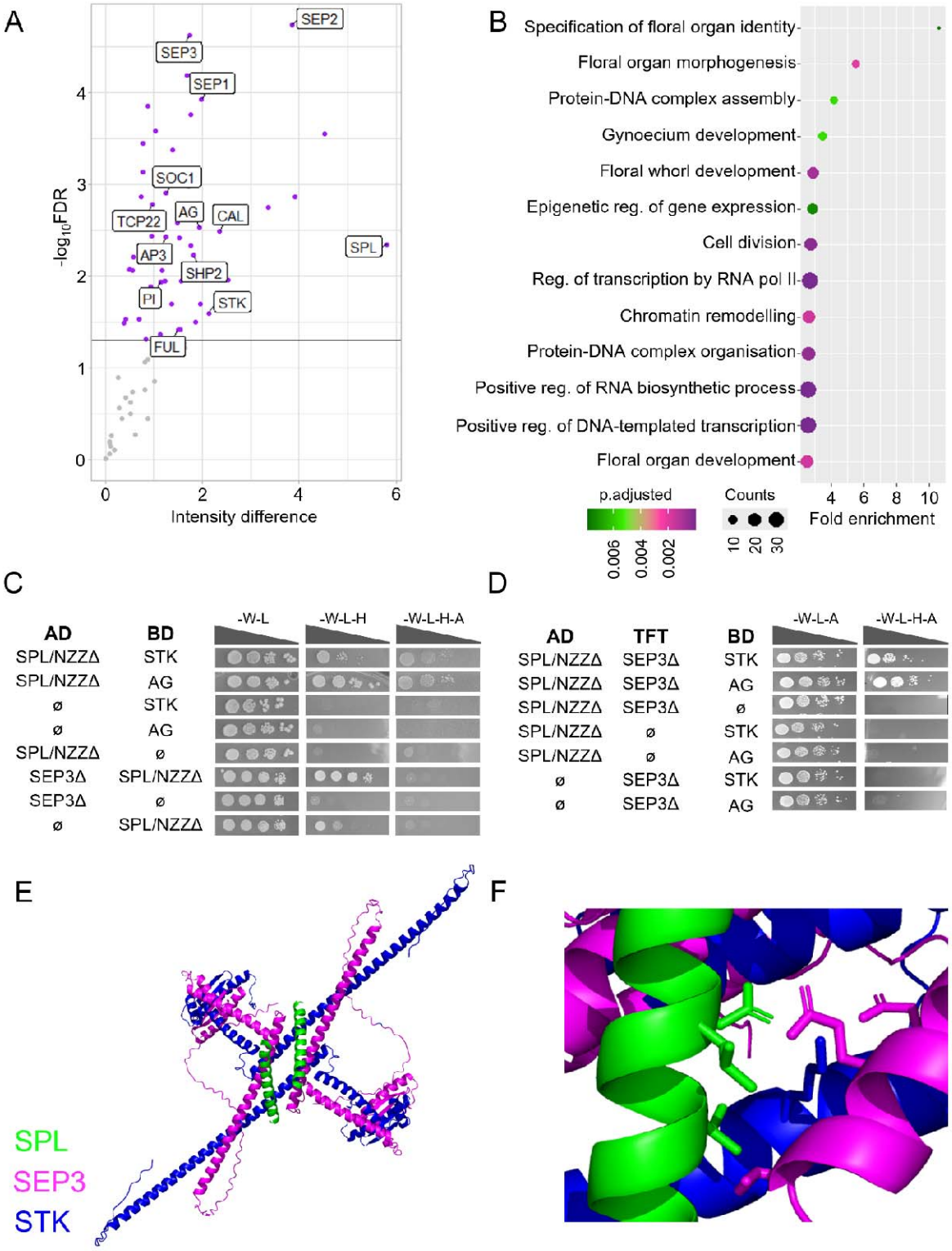
A
SEP2
SEP3
SEP1
SOC1
TCP22
AG
CAL
SPL
AP3
SHP2
PI
STK
FUL
-log10FDR
Intensity difference
B
Specification of floral organ identity
Floral organ morphogenesis
Protein-DNA complex assembly
Gynoecium development
Floral whorl development
Epigenetic reg. of gene expression
Cell division
Reg. of transcription by RNA pol II
Chromatin remodelling
Protein-DNA complex organisation
Positive reg. of RNA biosynthetic process
Positive reg. of DNA-templated transcription
Floral organ development
p.adjusted
Counts
Fold enrichment
C
AD
BD
-W-L
-W-L-H
-W-L-H-A
SPL/NZZΔ STK
SPL/NZZΔ AG
ø STK
ø AG
SPL/NZZΔ ø
SEP3Δ SPL/NZZΔ
SEP3Δ ø
ø SPL/NZZΔ
D
AD
TFT
BD
-W-L-A
-W-L-H-A
SPL/NZZΔ SEP3Δ STK
SPL/NZZΔ SEP3Δ AG
SPL/NZZΔ SEP3Δ ø
SPL/NZZΔ ø STK
SPL/NZZΔ ø AG
ø SEP3Δ STK
ø SEP3Δ AG
E
SPL
SEP3
STK
F

Figure 1. SPL/NZZ directly interacts with MADS-domain TFs. (**A**) Vulcano plot showing, with purple dots, the TFs statistically enriched in the SPL/NZZ Co-IP/MS dataset. MADS-domain TFs, SPL/NZZ and TCP22 have been highlighted with labels. The experiment has been performed using three independent biological replicates of *SPL/NZZ:GFP AP1:GR ap1cal* inflorescences at 9 DAI. Proteins with a positive enrichment (log_2 Intensity difference > 0) and FDR ≤ 0.05 were considered significant. (**B**) Biological process GO terms enrichment analysis of the SPL/NZZ putative direct interactors identified by Co-IP/MS. Enriched Go terms with an FDR ≤ 0.05 were considered significant (**C**) SPL/NZZ-MADS-domain TFs (AG, STK and SEP3) direct interaction by yeast-two-hybrid assay. Interactions are tested on media depleted of histidine (-W -L -H), or histidine and adenine (-W -L -H -A). For each interaction on the different media, yeast has been spotted at four different concentrations according to a serial dilution (OD 0.5; 1:10; 1:100; 1:1000). (**D**) SPL/NZZ form complexes with STK, SEP3 and AG by yeast-three-hybrid assays. Interactions are tested on a medium depleted of histidine (-W -L -H -A). For each interaction, yeast has been spotted at four different concentrations according to a serial dilution (OD 0.5; 1:10; 1:100; 1:1000). (**E**) AlphaFold3 predictions of the SPL/NZZ, SEP3 and STK complex. Two copies of STK are shown in blue, two copies of SEP3 are shown in magenta and two copies of SPL/NZZ aa61-91 are shown in green. (**F**) Close-up view of the (**E**) image, focusing on the SPL/NZZ motif (in green) and on the K domain of SEP3 (in magenta) and STK (in blue). The close-up view shows the residues that are at a maximum distance of 5 Å, which is the maximum distance for the establishment of hydrogen bond.

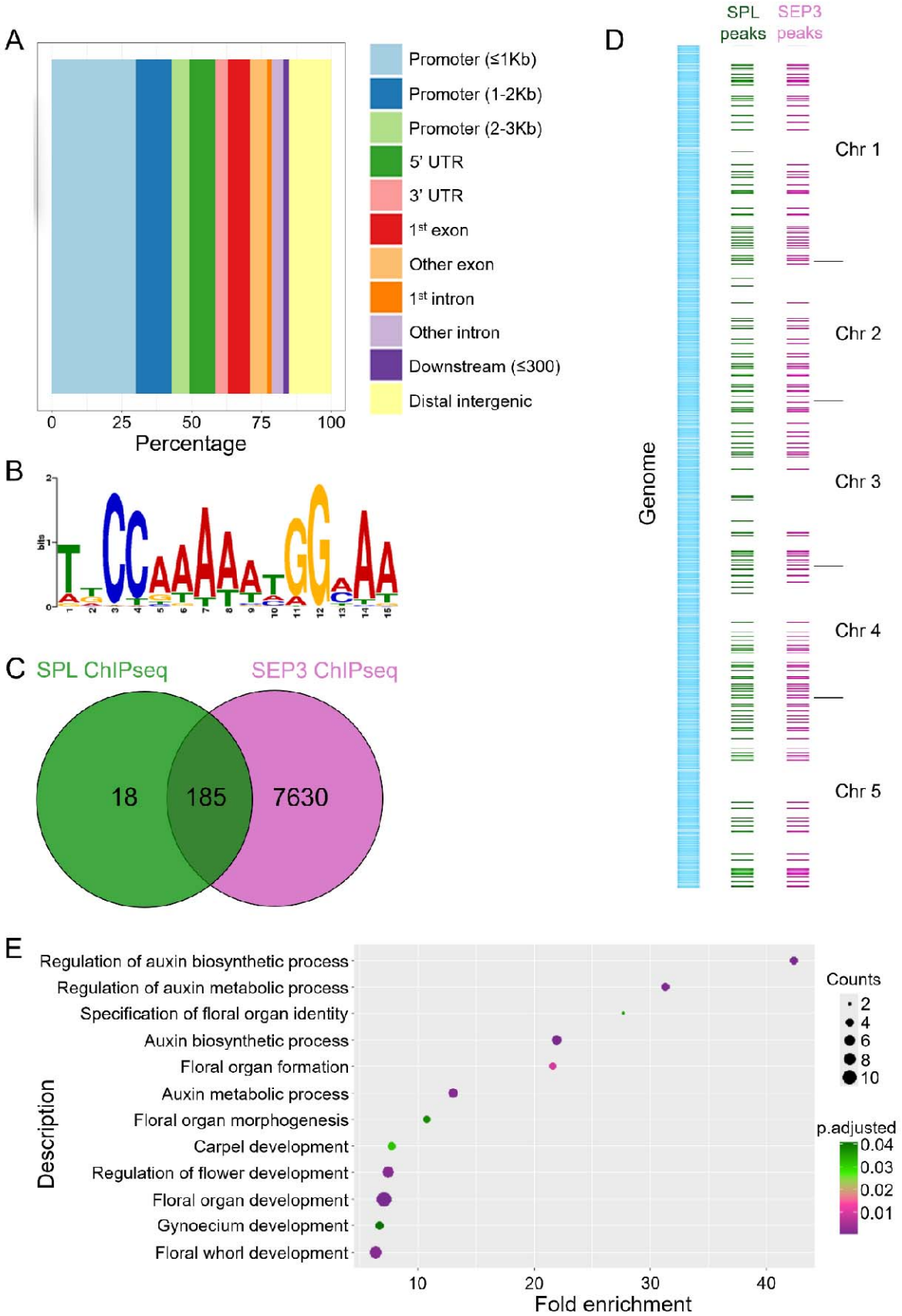
A
Promoter (≤1Kb)
Promoter (1-2Kb)
Promoter (2-3Kb)
5' UTR
3' UTR
1st exon
Other exon
1st intron
Other intron
Downstream (≤300)
Distal intergenic
0
25
50
75
100
Percentage
B
bits
C
SPL ChIPseq
SEP3 ChIPseq
18
185
7630
D
SPL peaks
SEP3 peaks
Genome
Chr 1
Chr 2
Chr 3
Chr 4
Chr 5
E
Regulation of auxin biosynthetic process
Regulation of auxin metabolic process
Specification of floral organ identity
Auxin biosynthetic process
Floral organ formation
Auxin metabolic process
Floral organ morphogenesis
Carpel development
Regulation of flower development
Floral organ development
Gynoecium development
Floral whorl development
Description
10
20
30
40
Fold enrichment
Counts
2
4
6
8
10
p.adjusted
0.04
0.03
0.02
0.01

968

Figure 2: SPL/NZZ direct target genes are shared with MADS-domain TFs. (**A**) Bar plot showing the SPL/NZZ ChIPseq peaks localisation along the genome. Around the 80% of the identified peaks falls in transcriptional regulatory sequences, such as promoter, 5' UTR, first exon, first intron and 3' UTR. The experiment has been performed on three biological replicates of *SPL/NZZ:GFP AP1:GR ap1cal* inflorescences at 9 DAI. Peaks were considered significant with FE> 0, FDR ≤ 0.05 and if present in at least 2 biological replicates out of 3. (**B**) The CArG-box motif is the only enriched TF DNA sequence binding-site identified among the SPL/NZZ ChIPseq peaks. The analysis has been performed with the XTREME tool from the MEME suite. (**C**) Venn diagram showing the intersection between the SPL/NZZ ChIPseq peaks and the SEP3 ChIPseq peaks. 185 SPL/NZZ peaks, representing more than 90% of the total peaks, are overlapping with SEP3 peaks. (**D**) SPL/NZZ ChIPseq and SEP3 ChIPseq overlapping peaks visualisation along the *A. thaliana* genome. All the significant SPL/NZZ ChIPseq peaks are visualized in green. SEP3 ChIPseq peaks overlapping with SPL/NZZ ones are shown in magenta. (**E**) Biological process GO term enrichment analysis, done on the 185 genes that have overlapping peaks between SPL/NZZ and SEP3 ChIPseq experiments. Categories associated to auxin and hormone processes, flower and floral organs development are enriched. Enriched GO terms with an FDR ≤ 0.05 were considered significant.

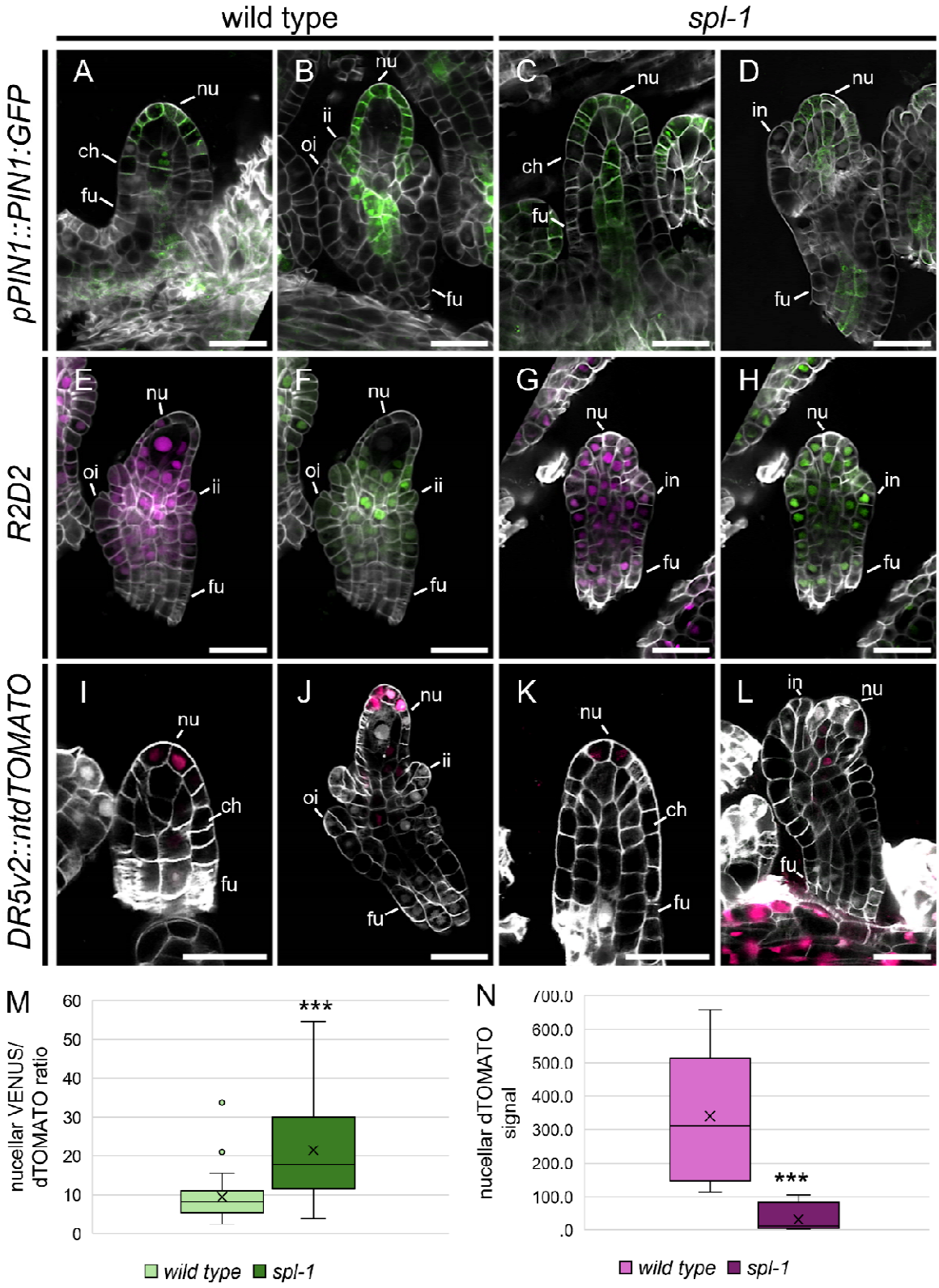
wild type
spl-1
pPIN1::PIN1:GFP
R2D2
DR5v2::ntdTOMATO
A
B
C
D
E
F
G
H
I
J
K
L
nu
ch
fu
ii
oi
in
M
N
nucellar VENUS/ dTOMATO ratio
nucellar dTOMATO signal
***
wild type
spl-1

999

1000

Figure 3: Auxin transport and signalling are impaired in the *spl-1* mutant ovule. (**A-D**) *pPIN1::PIN1:GFP* expression in wild type (**A**, **B**) and *spl-1* (**C**, **D**) ovules at stages 1-II (**A, C**) and 2-III (**B**, **D**). *PIN1* expression is severely impaired in the *spl-1* nucellus (**D**) with respect to the wild type (**B**) during the MMC differentiation stage. (**E**-**H**) *R2D2* reporter line in wild type (**E**, **F**) and *spl-1* (**G**, **H**) ovules at stage 2-III, showing mDII-tdTOMATO (**E**, **G**) and DII-VENUS (**F**, **H**) accumulation. Impairment in auxin transport in the *spl-1* ovule results in a reduce nucellar auxin level with respect to the wild type, as indicated by the DII-VENUS enhanced accumulation (**F**, **H**). (**I**-**L**) *DR5v2* expression in wild type (**I**, **J**) and *spl-1* (**K**, **L**) ovules at stages 1-II (**I**, **K**) and 2-III (**J**, **L**). The reduced auxin level in *spl-1* nucellus with respect to the wild type, results in a lower transcriptional output. (**M**) Box plot showing the tdTOMATO/VENUS signal ratio from the *R2D2* reporter, in the wild type and *spl-1* nucella. The analysis has been performed on 28 and 45 nuclei, from 3 wild type and 4 *spl-1* different ovules, respectively. Asterisks over boxes represent the statistical significance as determined by student's t-test, two-tailed distribution homoscedastic, confronting the mutant with the wild-type condition. *** = $p < 0.001$. (**N**) Box plot showing the nucellar tdTOMATO signal from the *DR5v2* reporter in the wild type and *spl-1* mutant. The analysis has been performed on 8 wild type and 11 *spl-1* different ovules. Asterisks over boxes represent the statistical significance as determined by student's t-test, two-tailed distribution homoscedastic, confronting the mutant with the wild-type condition. *** = $p < 0.001$. Box-plots elements correspond to: centre line = median; X = box limits = interquartile range; whiskers = lowest and highest values in the 1.5 interquartile range. Abbreviations: nu= nucella; ch= chalaza; fu= funiculus; ii= inner integument; oi= outer integument; in= integument. Scale Bars = 20 µm.

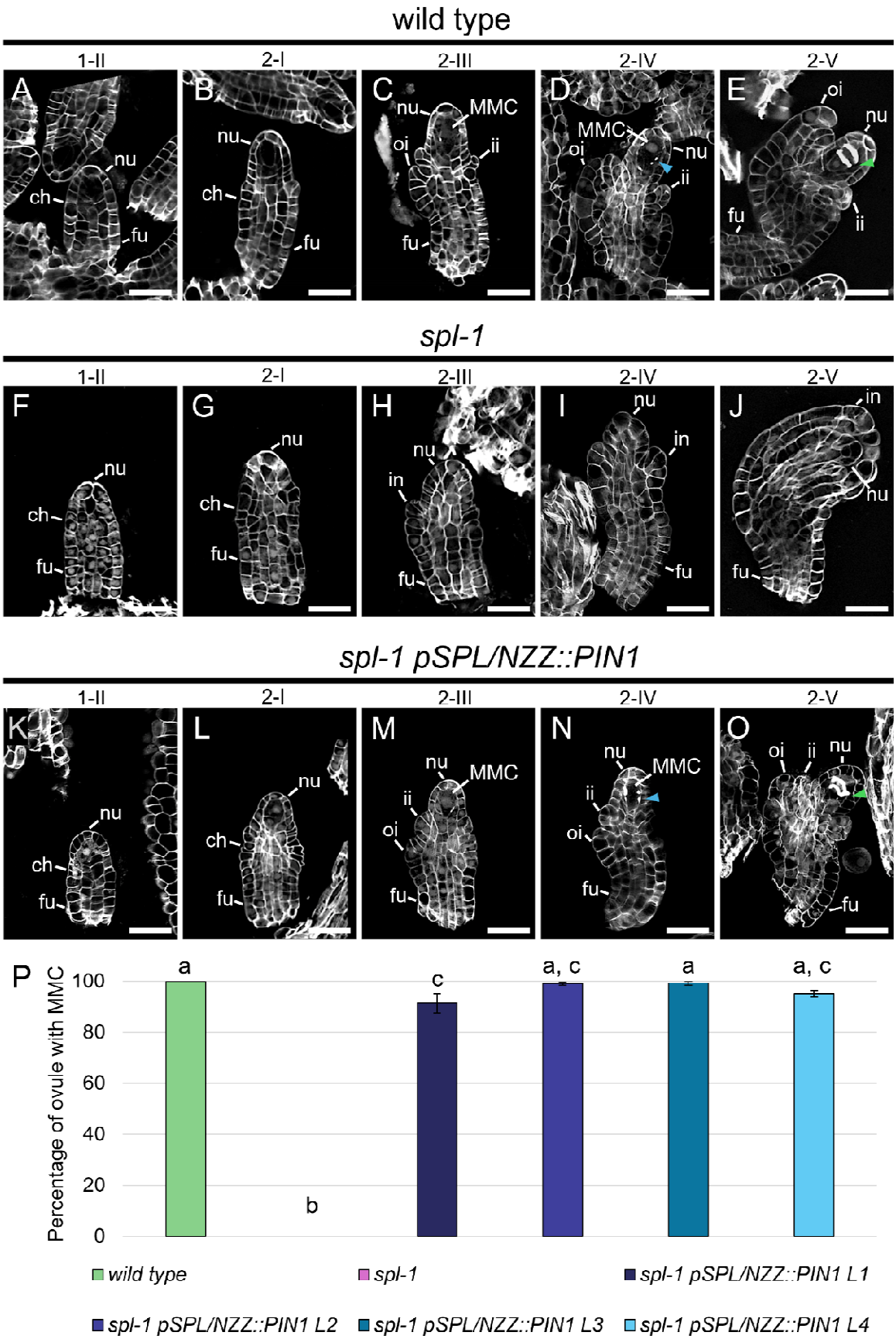
wild type
1-II
2-I
2-III
2-IV
2-V
A
B
C
D
E
nu
ch
fu
MMC
oi
ii
spl-1
F
G
H
I
J
in
spl-1 pSPL/NZZ::PIN1
K
L
M
N
O
P
Percentage of ovule with MMC
100
80
60
40
20
0
a
b
c
a, c
a
a, c
wild type
spl-1
spl-1 pSPL/NZZ::PIN1 L1
spl-1 pSPL/NZZ::PIN1 L2
spl-1 pSPL/NZZ::PIN1 L3
spl-1 pSPL/NZZ::PIN1 L4

Figure 4: PIN1 expression derived by *SPL/NZZ* regulatory sequences is sufficient to restore the MMC differentiation in the *spl-1* ovule. (**A-E**) wild type ovules at stage 1-II (**A**), 2-I (**B**), 2-III (**C**), 2-IV (**D**) and 2-V (**E**). At stage 2-III, the MMC is differentiated (**C**) while callose depositions can be observed at stage 2-IV (**D**). At stage 2-V (**E**), the MMC meiosis ends as denoted by the formation of the two meiotic plates. (**F-J**) *spl-1* ovules at stage 1-II (**F**), 2-I (**G**), 2-III (**H**), 2-IV (**I**) and 2-V (**J**). In the *spl-1* mutant the MMC do not differentiate (**H**, **I**). (**K-O**) *spl-1 pSPL/NZZ::PIN1* ovules at stage 1-II (**K**), 2-I (**L**), 2-III (**M**), 2-IV (**N**) and 2-V (**O**). Restoring *PIN1* expression in the *spl-1* nucellus is sufficient to drive the MMC differentiation (**M**, **N**). The MMC can be observed at stage 2-III (**M**). As in the wild-type situation (**D**) the MMC is surrounded by callose depositions at stage 2-IV (**N**) and correctly goes through the meiotic process (**O**). (**P**) Bar plot showing the mean ± SEM of the percentage of ovules developing the MMC, in wild type, *spl-1* and four *spl-1 pSPL/NZZ::PIN1* independent lines. The analysis has been performed on 8, 7, 8, 6, 8 and 9 different pistils, respectively, for the wild type (202 ovules observed in total), *spl-1* (238 ovules observed in total), *spl-1 pSPL/NZZ::PIN1 L1* (294 ovules observed in total), *spl-1 pSPL/NZZ::PIN1 L2* (196 ovules observed in total), *spl-1 pSPL/NZZ::PIN1 L3* (274 ovules observed in total) and *spl-1 pSPL/NZZ::PIN1 L4* (364 ovules observed in total). Letters above the bars indicate homogenous categories with $p < 0.05$ as determined by one-way ANOVA with post-hoc Tukey HSD test. Abbreviations: nu= nucella; ch= chalaza; fu= funiculus; ii= inner integument; oi= outer integument; in= integument; MMC= megaspore mother cell. Blue arrowheads indicate the callose depositions. Green arrowhead indicates the meiotic plates. Scale bar = 20 µm

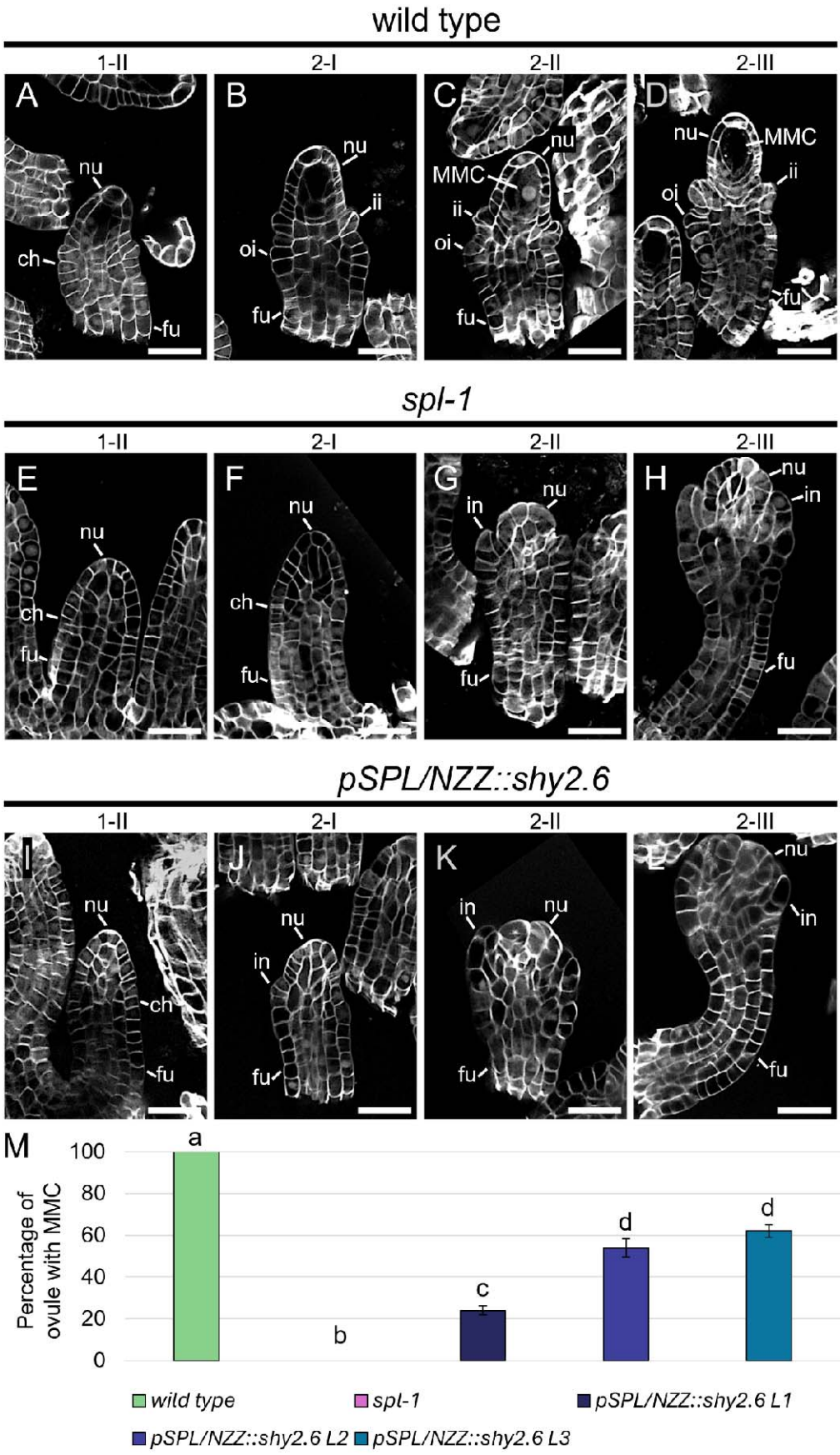
wild type
1-II
2-I
2-II
2-III
A
B
C
D
nu
ch
fu
ii
oi
MMC
spl-1
E
F
G
H
in
pSPL/NZZ::shy2.6
I
J
K
L
M
Percentage of ovule with MMC
100
80
60
40
20
0
a
b
c
d
d
wild type
spl-1
pSPL/NZZ::shy2.6 L1
pSPL/NZZ::shy2.6 L2
pSPL/NZZ::shy2.6 L3

Figure 5: *shy2.6* expression in the nucellus impair the MMC differentiation. (**A-D**) wild type ovules at stage 1-II (**A**), 2-I (**B**), 2-II (**C**) and 2-III (**D**). (**E**-**H**) *spl-1* ovules at stage 1-II (**E**), 2-I (**F**), 2-II (**G**) and 2-III (**H**). (**I**-**L**) *pSPL/NZZ:shy2.6* ovules at stage 1-II (**I**), 2-I (**J**), 2-II (**K**) and 2-III (**L**). *shy2.6* expression in the wild-type nucellus impair the MMC differentiation, mimicking the *spl-1* phenotype (**G**, **H, K**, **L**). (**M**) Bar plot showing the mean ± SEM of the percentage of ovules showing an MMC in wild type, *spl-1* and *pSPL/NZZ::shy2.6* lines. The analysis has been performed on 3, 4, 8, 9 and 5 different pistils, respectively, for the wild type (113 ovules observed in total), *spl-1* (157 ovules observed in total), *pSPL/NZZ::shy2.6 L1* (356 ovules observed in total), *pSPL/NZZ::shy2.6 L2* (378 ovules observed in total) and *spl-1 pSPL/NZZ::shy2.6* L3 (202 ovules observed in total). Letters above the bars indicate homogenous categories with $p < 0.05$, as determined by one-way ANOVA with post-hoc Tukey HSD test. Abbreviations: nu= nucella; ch= chalaza; fu= funiculus; ii= inner integument; oi= outer integument; in= integument; MMC= megaspore mother cell. Scale bars = 20µm.

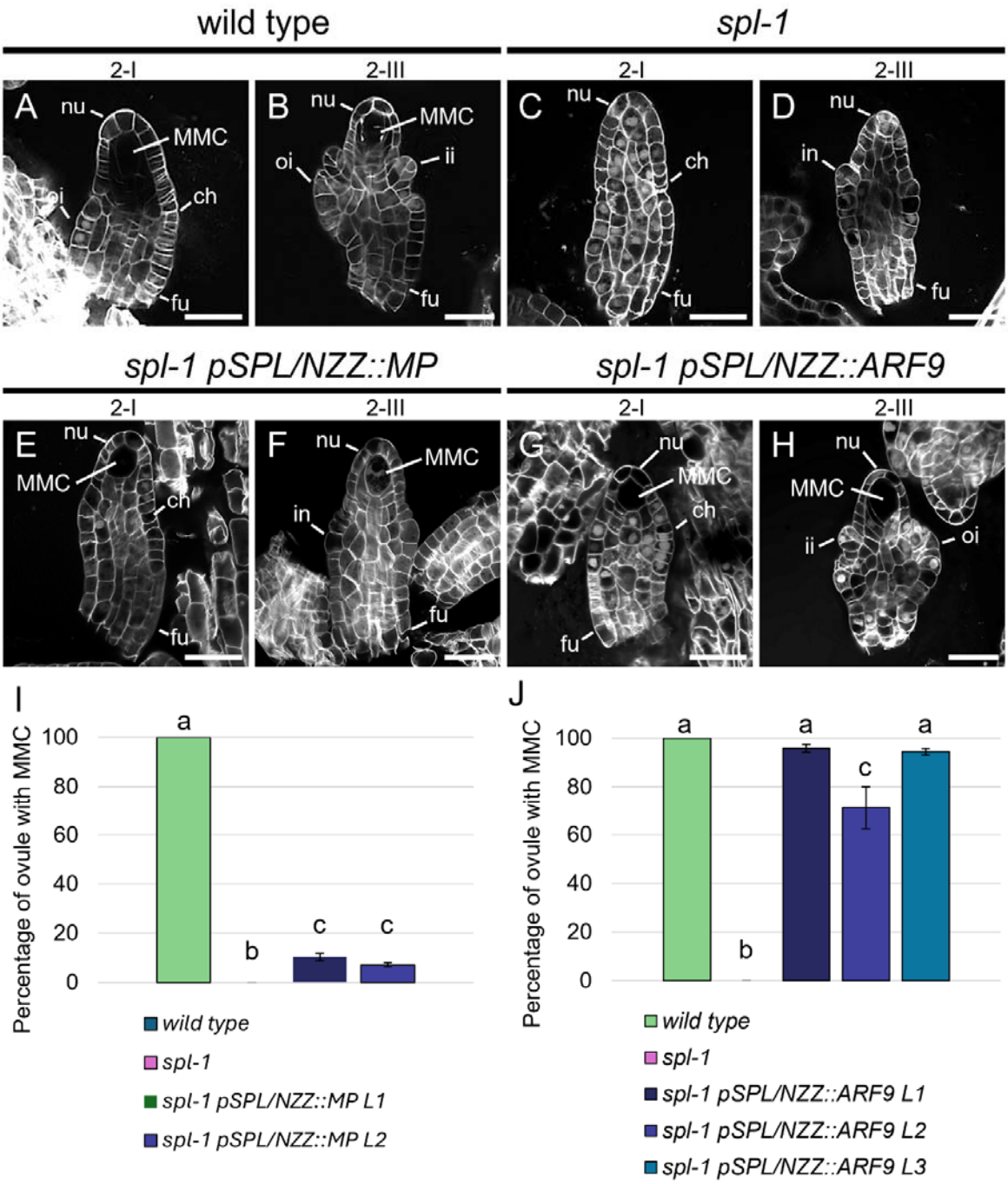

1094

1095

1096

1097

1098

Figure 6: Increase ARF levels in the *spl-1* nucellus partially restore the MMC differentiation. (**A, B**) wild type ovules at stage 2-I (**A**) and 2-III (**B**). (**C, D**) *spl-1* ovules at stage 2-I (**C**) and 2-III (**D**). (**E**, **F**) *spl-1 pSPL/NZZ::MP* ovules at stage 2-I (**E**) and 2-III (**F**). (**G**, **H**) *spl-1 pSPL/NZZ::ARF9* ovules at stage 2-I (**G**) and 2-III (**H**). While increasing *MP* expression only partially restores the MMC differentiation, *pSPL/NZZ::ARF9* rescues the MMC differentiation in *spl-1* (**I**) Bar plot showing the mean ± SEM of the percentage of ovules showing an MMC in wild type, *spl-1* and *spl-1 pSPL/NZZ::MP* lines. The analysis has been performed on 5, 8, 12 and 9 different pistils for the wild type (150 ovules observed in total), *spl-1* (304 ovules observed in total), *spl-1 pSPL/NZZ::MP L1* (362 ovules observed in total) and *spl-1 pSPL/NZZ::MP L2* (270 ovules observed in total). Letters above the bars indicate homogenous categories with $p < 0.05$, as determined by one-way ANOVA with post-hoc Tukey HSD test. (**J**) Bar plot showing the mean ± SEM of the percentage of ovules showing an MMC in wild type, *spl-1* and *spl-1 pSPL/NZZ::ARF9* lines. The analysis has been performed on 4, 4, 5, 4, 4 different pistils for the wild type (157 ovules observed in total), *spl-1* (131 ovules observed in total), *spl-1 pSPL/NZZ::ARF9 L1* (193 ovules observed in total), *spl-1 pSPL/NZZ::ARF9 L2* (115 ovules observed in total) and *spl-1 pSPL/NZZ::ARF9 L3* (177 ovules observed in total). Letters above the bars indicate homogenous categories with $p < 0.05$, as determined by one-way ANOVA with post-hoc Tukey HSD test. Abbreviations: nu= nucella; ch= chalaza; fu= funiculus; ii= inner integument; oi= outer integument; in= integument; MMC= megaspore mother cell. Scale bars = 20µm.

1129

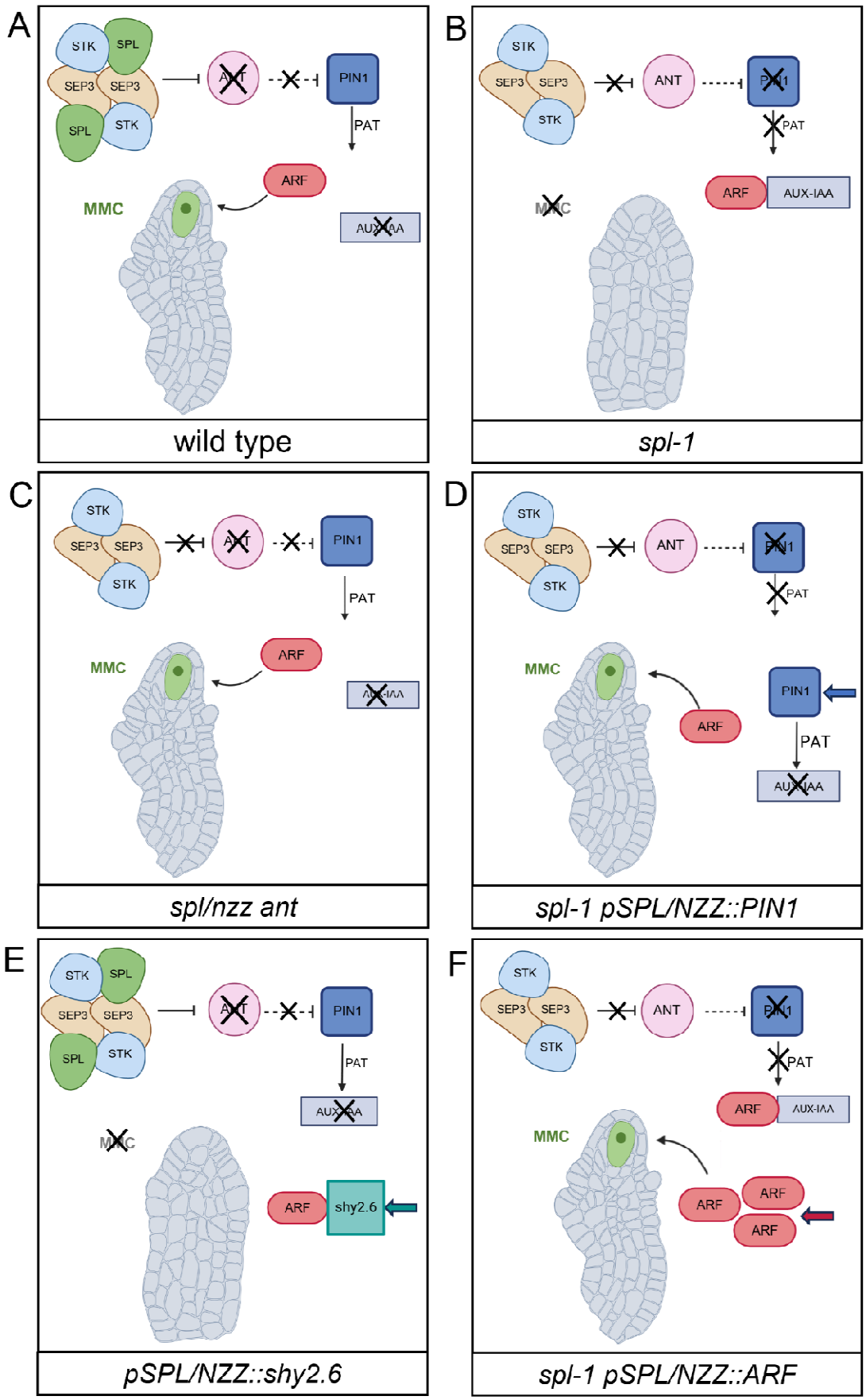
A
STK
SPL
SEP3
SEP3
SPL
STK
ANT
PIN1
PAT
ARF
MMC
AUX-IAA
wild type
B
STK
SEP3
SEP3
STK
ANT
PIN1
PAT
ARF
AUX-IAA
MMC
spl-1
C
STK
SEP3
SEP3
STK
ANT
PIN1
PAT
ARF
MMC
AUX-IAA
spl/nzz ant
D
STK
SEP3
SEP3
STK
ANT
PIN1
PAT
MMC
ARF
PIN1
PAT
AUX-IAA
spl-1 pSPL/NZZ::PIN1
E
STK
SPL
SEP3
SEP3
SPL
STK
ANT
PIN1
PAT
AUX-IAA
MMC
ARF
shy2.6
pSPL/NZZ::shy2.6
F
STK
SEP3
SEP3
STK
ANT
PIN1
PAT
ARF
AUX-IAA
MMC
ARF
ARF
ARF
spl-1 pSPL/NZZ::ARF

Figure 7: SPL/NZZ, by indirectly regulating *PIN1* expression, determine the MMC differentiation though an auxin-dependent network. (**A**) In the wild type, SPL/NZZ interacts with the ovule-identity MADS-domain complex to inhibit *ANT* expression, facilitating auxin accumulation in the nucellus and subsequently enabling the ARF-mediated auxin response required to promote the MMC specification. (**B**) In the *spl/nzz* mutant, *ANT* is expressed in the nucellus, leading to the downregulation of *PIN1* and to an auxin subthreshold concentration, which disable the post-translational activation of the ARFs, necessary for MMC formation**.** (**C**) In the *ant spl/nzz* mutant, the inhibition of *PIN1* does not take place, allowing the formation of the MMC even in the absence of SPL/NZZ. (**D**) Expressing *PIN1* under the control of the *SPL/NZZ* promoter in the *spl/nzz* mutant, is sufficient to restore the proper auxin threshold in the nucellus and the ARF-mediated auxin response required for the MMC specification. (**E**) The expression of the non-degradable *shy2.6* isoform in the wild-type nucellus leads to the post-translational deactivation of the ARFs, resulting in the absence of the MMC formation. (**F**) Increase ARF levels in the *spl/nzz* mutant can overcome the repressive state caused by AUX/IAAs over-accumulation, determining the MMC differentiation.

Supplementary Figures

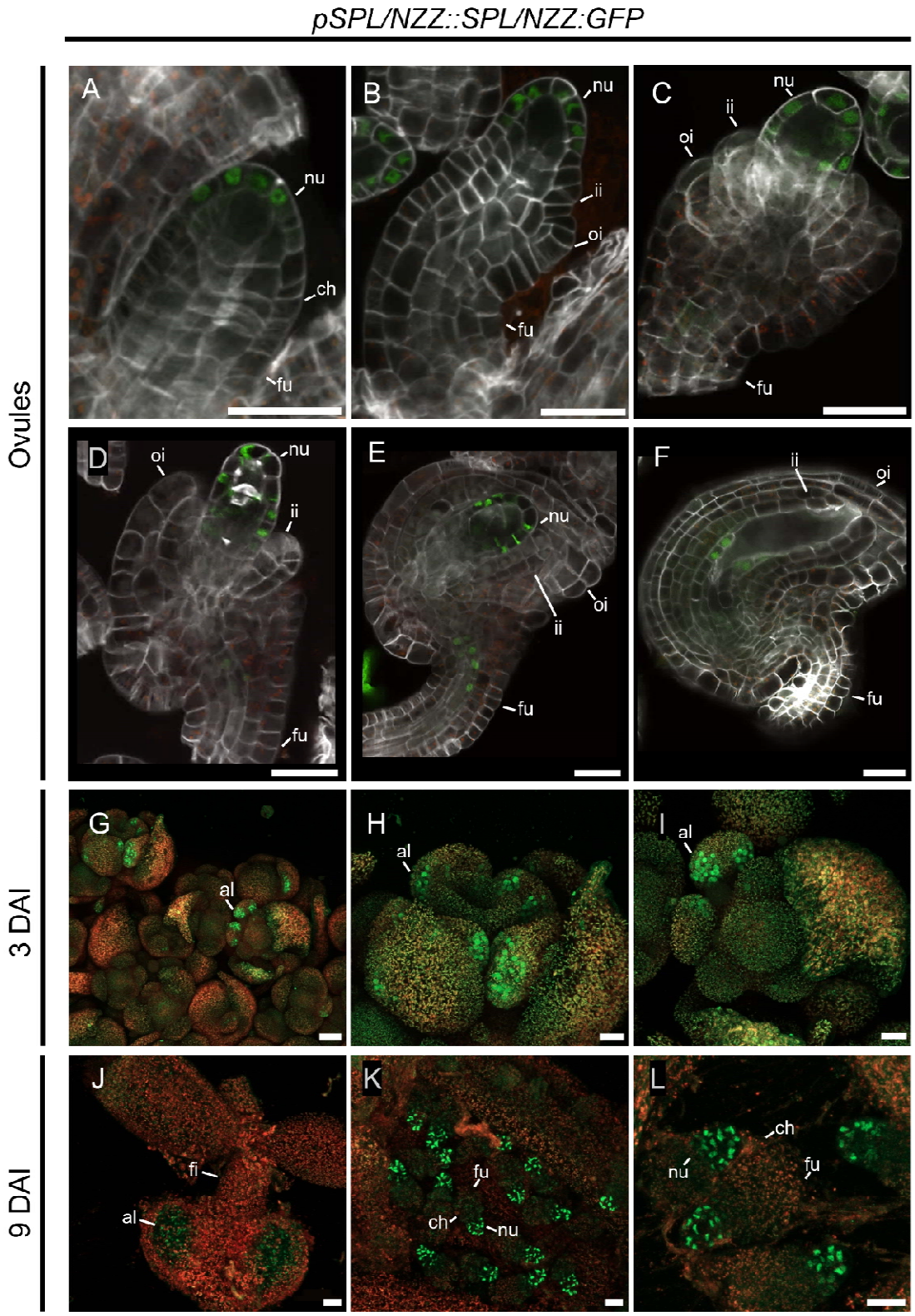

Supplementary Figure 1: *pSPL/NZZ::SPL/NZZ:GFP* expression. (**A-F**) *pSPL/NZZ::SPL/NZZ:GFP* expression during different stages of ovule development. SPL/NZZ is localised in the apical L1 cells at stages 1-II (**A**) and 2-II (**B**). At stage 2-IV (**C**) and 2-V (**D**), SPL/NZZ accumulates in whole nucellar L1 layer. At stage 3-I (**E**), SPL/NZZ is present in the L1 layer and in the central part of the funiculus. At ovule maturity (**F**), the L1 layer degenerates and SPL/NZZ accumulates in the remaining cells. (**G-I**) *pSPL/NZZ::SPL/NZZ:GFP* expression in *pAP1::AP1:GR ap1cal* inflorescences at 3 DAI. At 3 DAI, SPL/NZZ-GFP signal is visible only in developing anthers. (**J-L**) *pSPL/NZZ:SPL/NZZ:GFP* expression in *pAP1::AP1:GR ap1cal* inflorescences at 9 DAI. At 9 DAI, SPL/NZZ-GFP is not visible in anthers anymore (**J**). By contrast, SPL/NZZ-GFP strongly accumulates in ovules nucella (**K, L**). Abbreviations: nu= nucella; ch= chalaza; fu= funiculus; ii= inner integument; oi= outer integument; al= anther lobe; fi= filament. (**A-F, H-L**) Scale bar = 20 µm. (**G**) Scale bar = 50 µm.

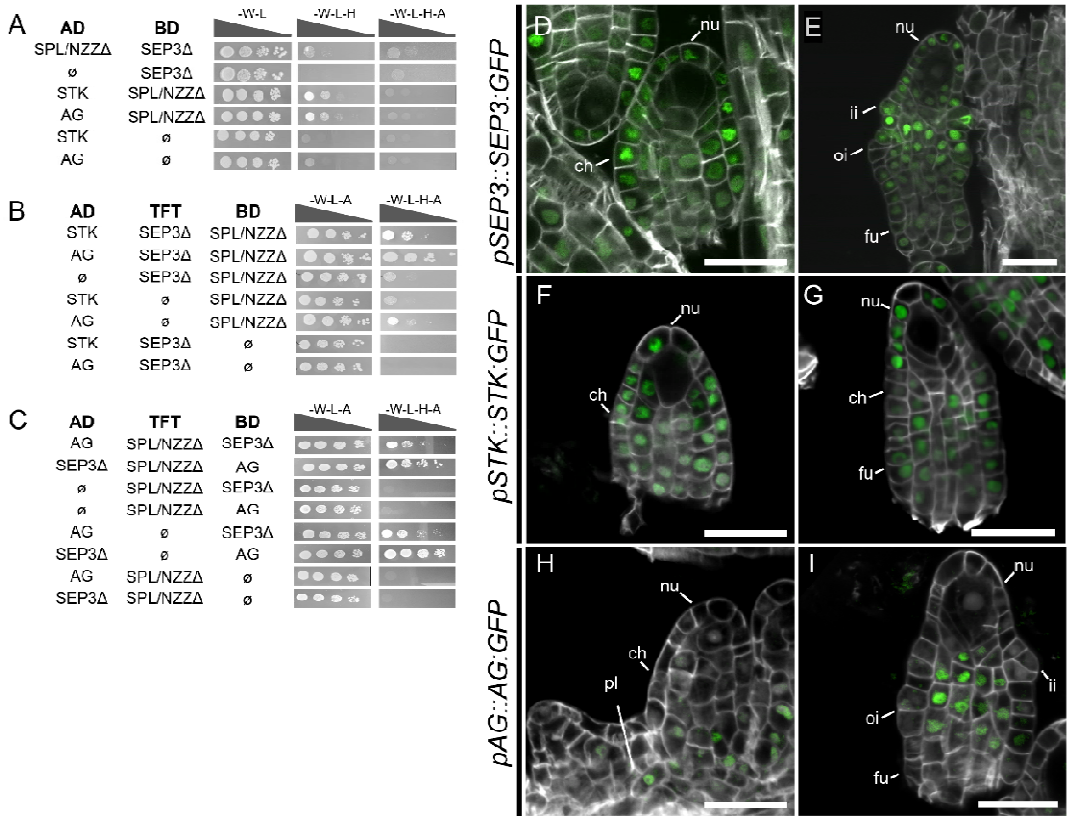

Supplementary Figure 2: Results of yeast-two- and three-hybrid assays and SEP3, STK and AG accumulation patterns in the ovule. (**A**) Yeast-two-hybrid assay showing interaction between SPL/NZZ and MADS-domain TFs (SEP3, STK, AG). The controls are shown in the Figure 1C. Interactions are tested on media depleted of histidine (-W -L -H), or histidine and adenine (-W -L -H -A). For each interaction on the different media, yeast has been spotted at four different concentrations according to a serial dilution (OD 0,5; 1:10; 1:100; 1:1000). (**B, C**) Yeast-three-hybrid assay showing the formation of SPL/NZZ, STK and SEP3 complex, by fusing SPL/NZZ either to the GAL4 BD (**B**) or to the TFT (**C**)**.** Interactions are tested on a medium depleted of histidine (-W -L -H -A). For each interaction, yeast has been spotted at four different concentrations according to a serial dilution (OD 0,5; 1:10; 1:100; 1:1000). (**D, E**) *pSEP3::SEP3:GFP* reporter line showing SEP3 accumulation in ovules at stage 2-I (**D**) and 2-III (**E**). (**F, G**) *pSTK::STK:GFP* reporter line in ovules at stage 2-I (**F**) and 2-II (**G**)**.** (**H, I**) *pAG::AG:GFP* reporter line in ovules at stage 2-I (**H**) and 2-II (**I**)**.** Abbreviations: nu= nucella; ch= chalaza; fu= funiculus; ii= inner integument; oi= outer integument; pl= placenta. Scale bar = 20 µm.

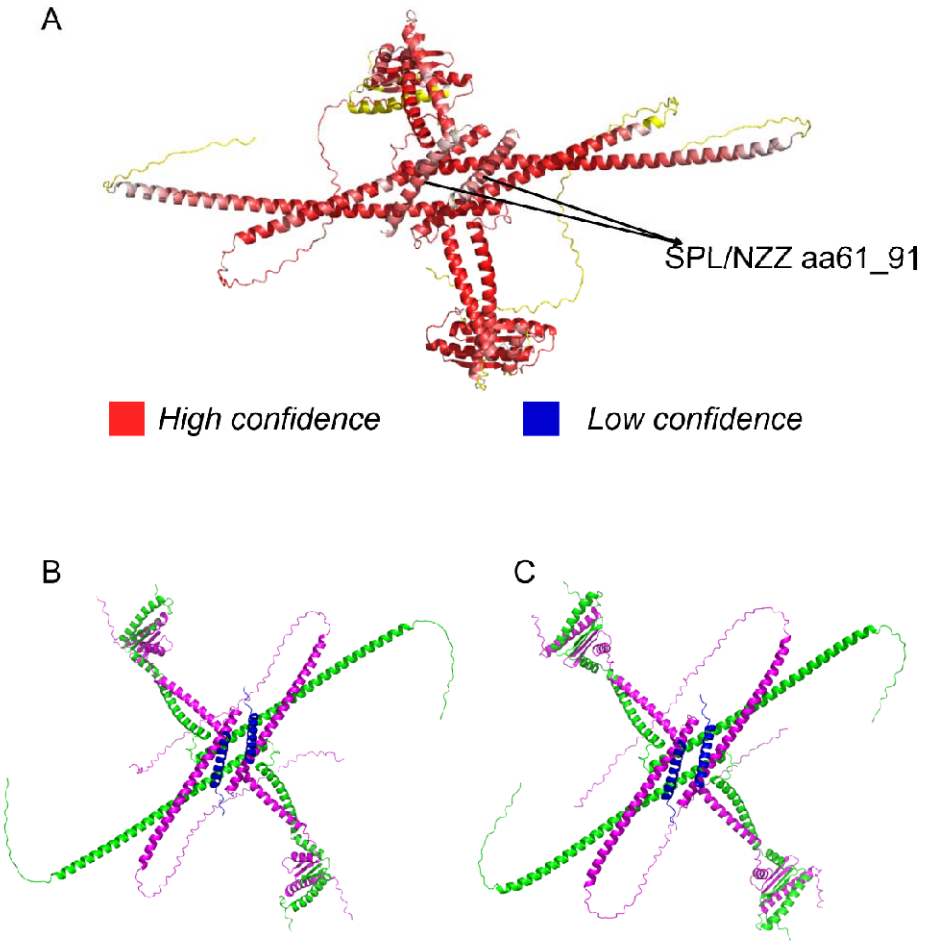

Supplementary Figure 3: AplhaFold3 predictions of SPL/NZZ-SEPs-STK complexes. (**A**) SPL/NZZ-SEP3-STK complex prediction coloured according to the prediction confidence. Red colours represent a high confidence, while blue colour a low confidence. (**B**) Prediction of the complex made by two copies of STK (in green), two copies of SPL/NZZaa61-91 (in blue) and two copies of SEP1 (in magenta). (**C**) prediction of the complex made by two copies of STK (in green), two copies of SPL/NZZaa61-91 (in blue) and two copies of SEP2 (in magenta).

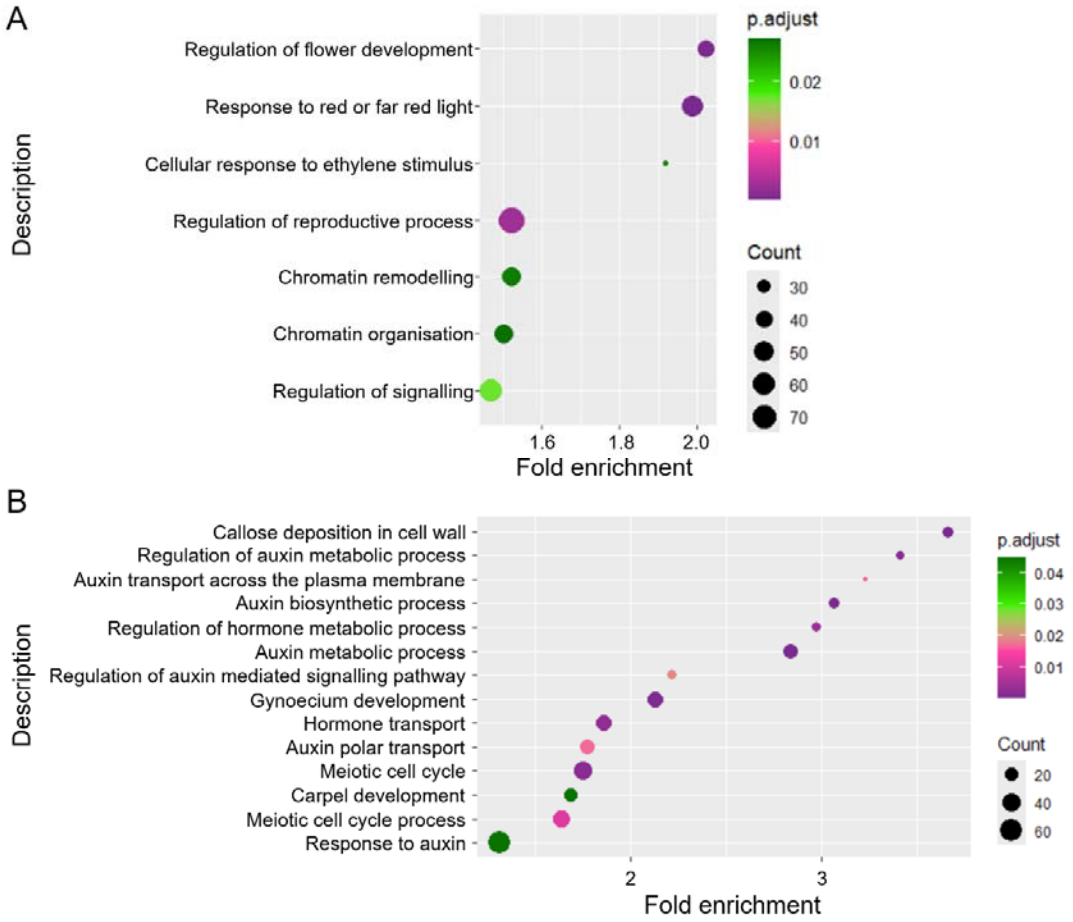

Supplementary Figure 4: Biological processes GO terms enrichment analysis of DE genes in the *spl-1* pistil with respect to the wild type. (**A**) Biological process GO terms enrichment analysis conducted on the downregulated genes in *spl-1* pistils with respect to wild type. Categories associated to flower development and chromatin organisation are among the most enriched categories. (**B**) Biological process GO terms enrichment analysis conducted on the upregulated genes in *spl-1* pistils with respect to wild type. Categories associated to meiosis, gynoecium development, auxin and hormones processes are among the most enriched categories.

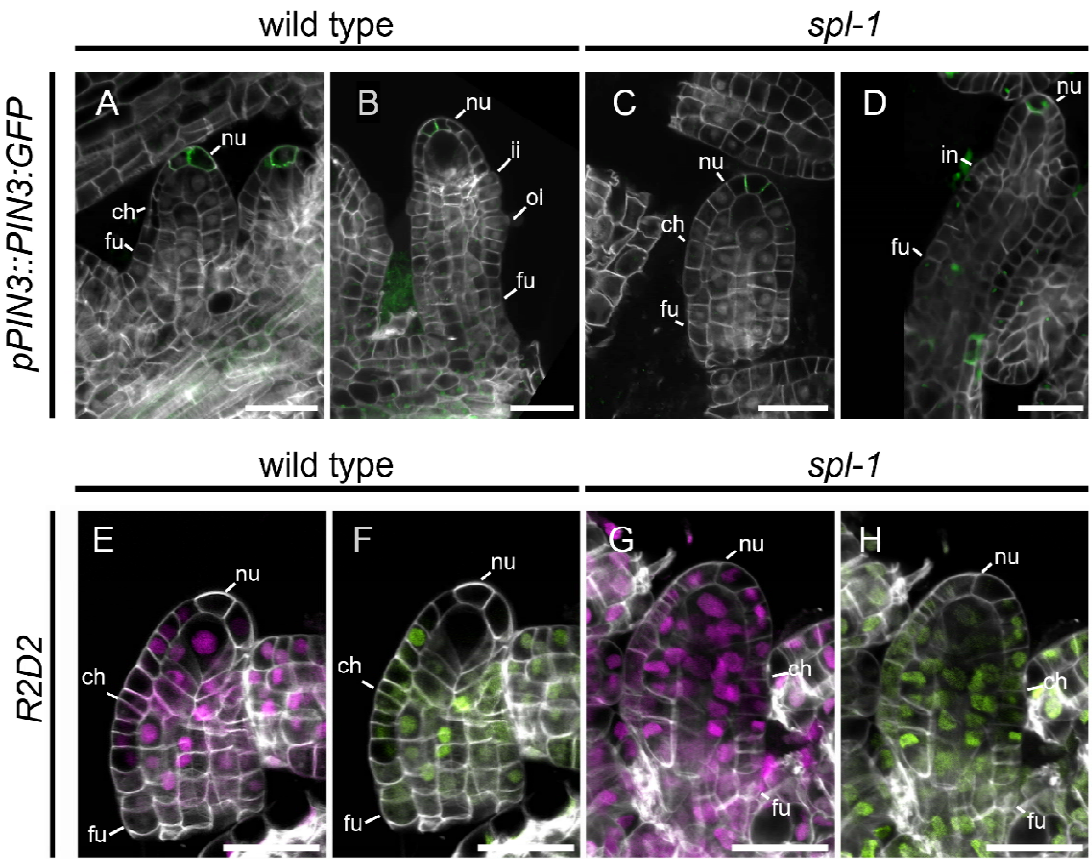

Supplementary Figure 5: *pPIN3::PIN3:GFP* expression in wild type and *spl-1* ovules and *R2D2* signal in wild type and *spl-1* ovules at stage 1-II. (**A, B**) PIN3-GFP accumulation at stage 2-I (**A**) and 2-II (**B**) in wild type. (**C, D**) PIN3-GFP accumulation at stage 2-I (**C**) and 2-II (**D**) in *spl-1*. (**E-H**) *R2D2* reporter line in wild type (**E**, **F**) and *spl-1* (**G**, **H**) ovules at stage 1-II, showing mDII-tdTOMATO (**E**, **G**) and DII-VENUS (**F**, **H**) accumulation. Abbreviations: nu= nucellus; ch= chalaza; fu= funiculus; ii= inner integument; oi= outer integument; in= integument. Scale bar = 20 µm.

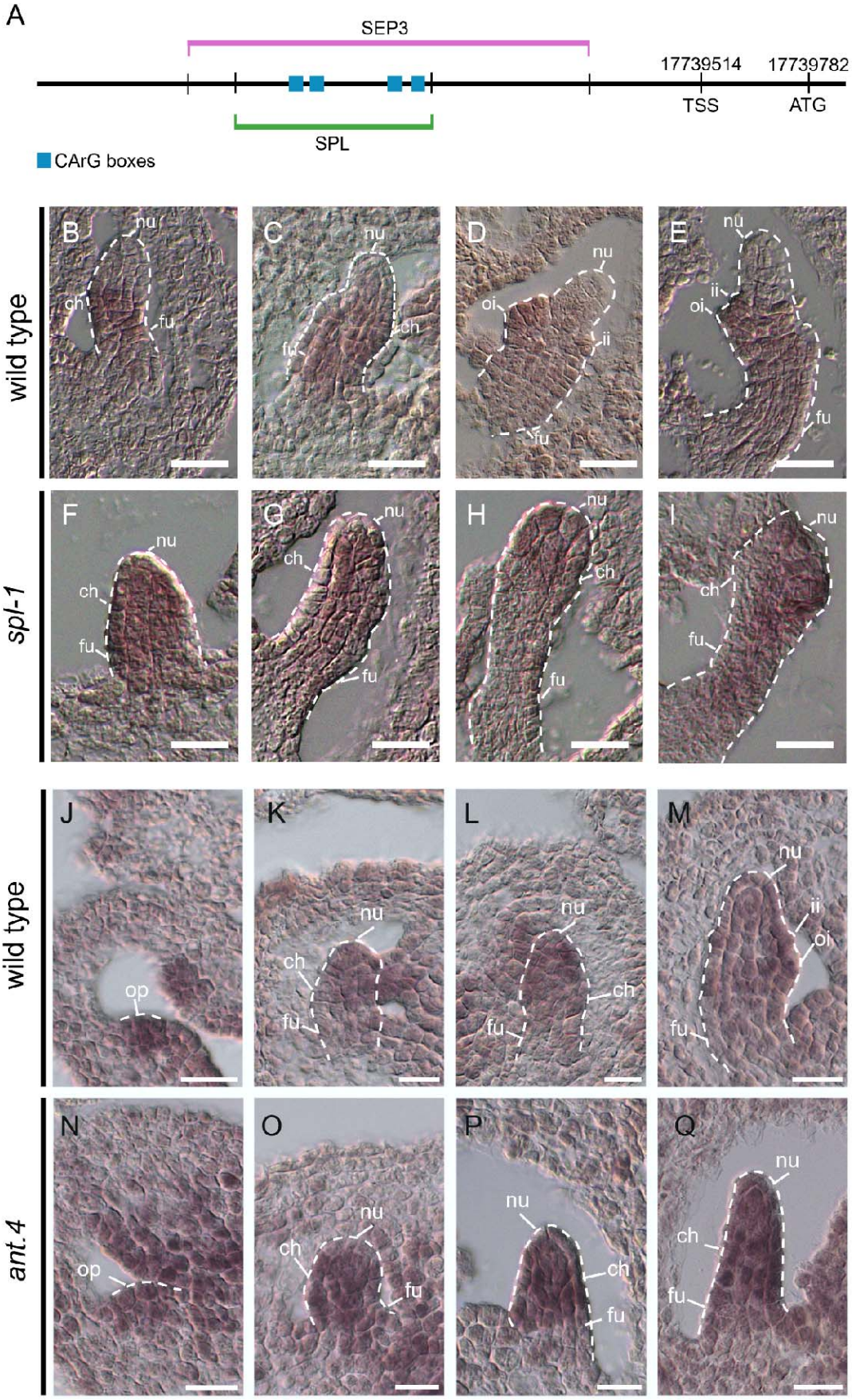
A
SEP3
17739514
17739782
TSS
ATG
SPL
CArG boxes
wild type
spl-1
wild type
ant.4
B
C
D
E
F
G
H
I
J
K
L
M
N
O
P
Q
nu
ch
fu
oi
ii
op

1243

Supplementary Figure 6: SPL/NZZ and SEP3 ChIPseq peaks on *ANT* promoter, *ANT* expression in wild type and *spl-1* ovules and *PIN1* expression in wild type and *ant.4* ovules. (**A**) Schematic of the *ANT* promoter region showing, with a green box, the peak identified in the SPL/NZZ ChIPseq and in magenta the peak identified in the SEP3 ChIPseq. The 4 CArG-box sequences identified by the MEME analysis on the SPL/NZZ peak are highlighted by blue boxes. (**B**-**I**) *ANT* transcript *in-situ* hybridisation on wild type (**B-E**) and *spl-1* (**F-I**) ovules. In wild-type ovules, *ANT* is expressed in the chalaza and the funiculus (**B-E**) whereas, *ANT* transcript accumulates ectopically also in the nucellus in the *spl-1* mutant (**F-I**). (**J**-**Q**) *PIN1* expression detected by *in-situ* hybridisation in wild type (**J**-**M**) and *ant.4* (**N**-**Q**) ovules at stages 1-I (**J**, **N**), 1-II (**K**, **O**), 2-I (**L**, **P**) and 2-III (**M**, **Q**). At stages 2-I, *PIN1* expression could be observed mainly in the nucellus of the wild-type ovule (**L**). At stage 2-III (**M**), *PIN1* is still visible in the nucellus and partially in the chalaza. By contrast, in the *ant.4* ovule (**N**-**Q**), *PIN1* expression can be observed in the whole ovule primordia. Abbreviations: op= ovule primordia; nu= nucellus; ch= chalaza; fu= funiculus; ii= inner integument; oi= outer integument. Scale bars = 20µm.

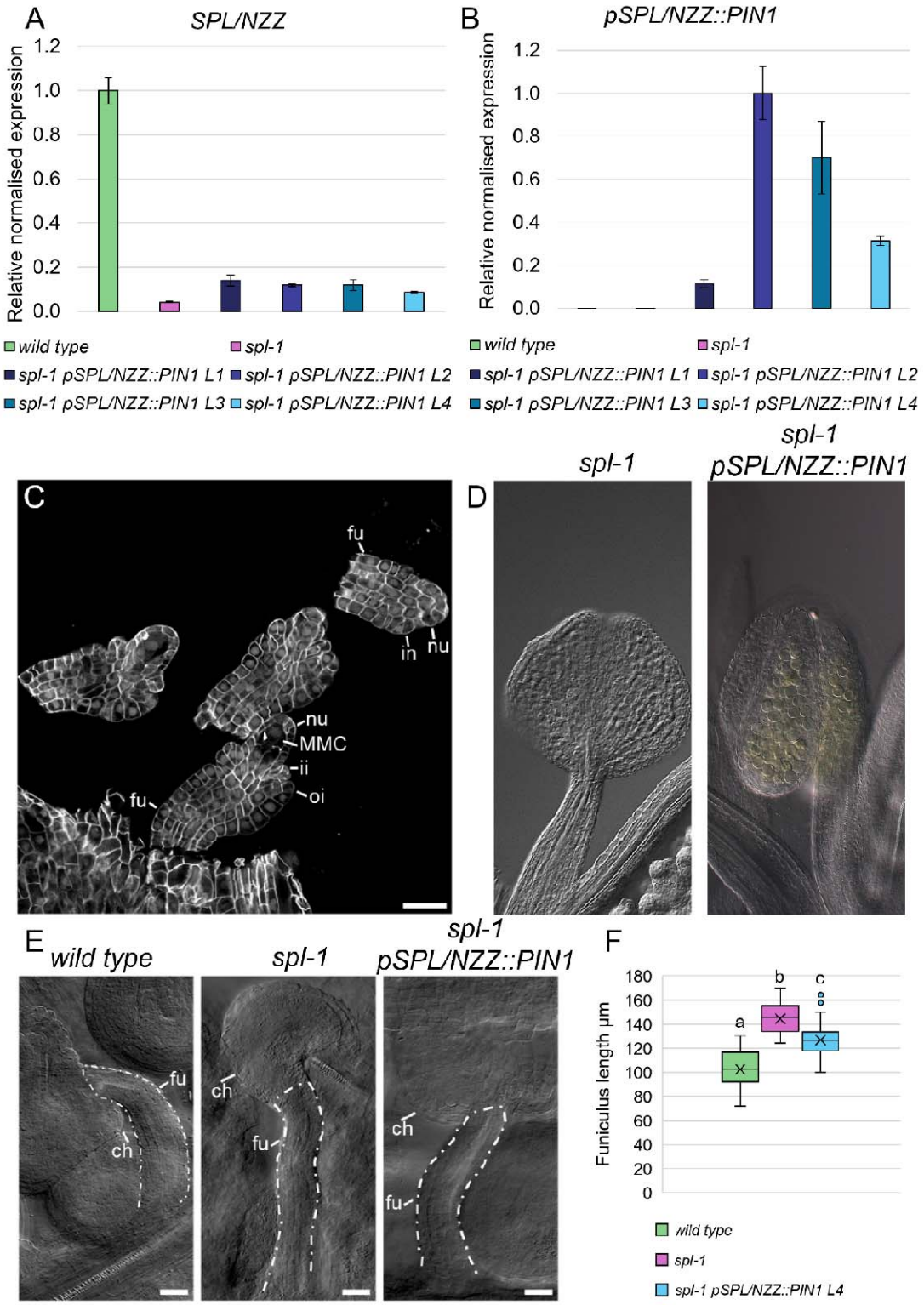

1273

1274

1275

1276

Supplementary Figure 7: *pSPL/NZZ::PIN1* expression and phenotypes of the *spl-1 pSPL/NZZ::PIN1* plants. (**A**) Bar plot showing *SPL/NZZ* relative normalised expression in inflorescences from the wild type, *spl-1* and four independent *spl-1 pSPL/NZZ::PIN1* lines. (**B**) Bar plot showing *pSPL/NZZ::PIN1* relative normalised expression in the same samples presented in (**A**). *ACTIN8* was used as the housekeeping gene. Bars represent the mean ± SEM of the expression, as evaluated from three technical replicates per each sample. (**C**) Despite the ability of *pSPL/NZZ::PIN1* to rescue the MMC specification, few ovules still resembles the *spl-1* phenotype. (**D**) *spl-1* and *spl-1 pSPL/NZZ::PIN1* anthers. In contrast to the *spl-1* situation, *spl-1 pSPL/NZZ::PIN1* could develop anthers generating wild-type-like pollen grains. (**E**, **F**) Funiculus length in wild type, *spl-1* and *spl-1 pSPL/NZZ::PIN1* ovules at stage 3-VI. Even though the ovule development was restored in *spl-1 pSPL/NZZ::PIN1,* funiculi were still statistically longer than the wild-type ones. Nevertheless, *spl-1 pSPL/NZZ::PIN1* funiculi resulted statistically shorter than the *spl-1* ones (**F**). Measurements were performed on 25, 33 and 45 different funiculi, respectively, for the wild type, *spl-1* and *spl-1 pSPL/NZZ::PIN1 L4.* Letters above the box plots indicate homogenous categories with $p < 0.05$, as determined by one-way ANOVA with post-hoc Tukey HSD test. Box-plots elements correspond to: centre line = median; X= average; box limits = interquartile range; whiskers = lowest and highest values in the 1.5 interquartile range. Scale bars = 20 µm.

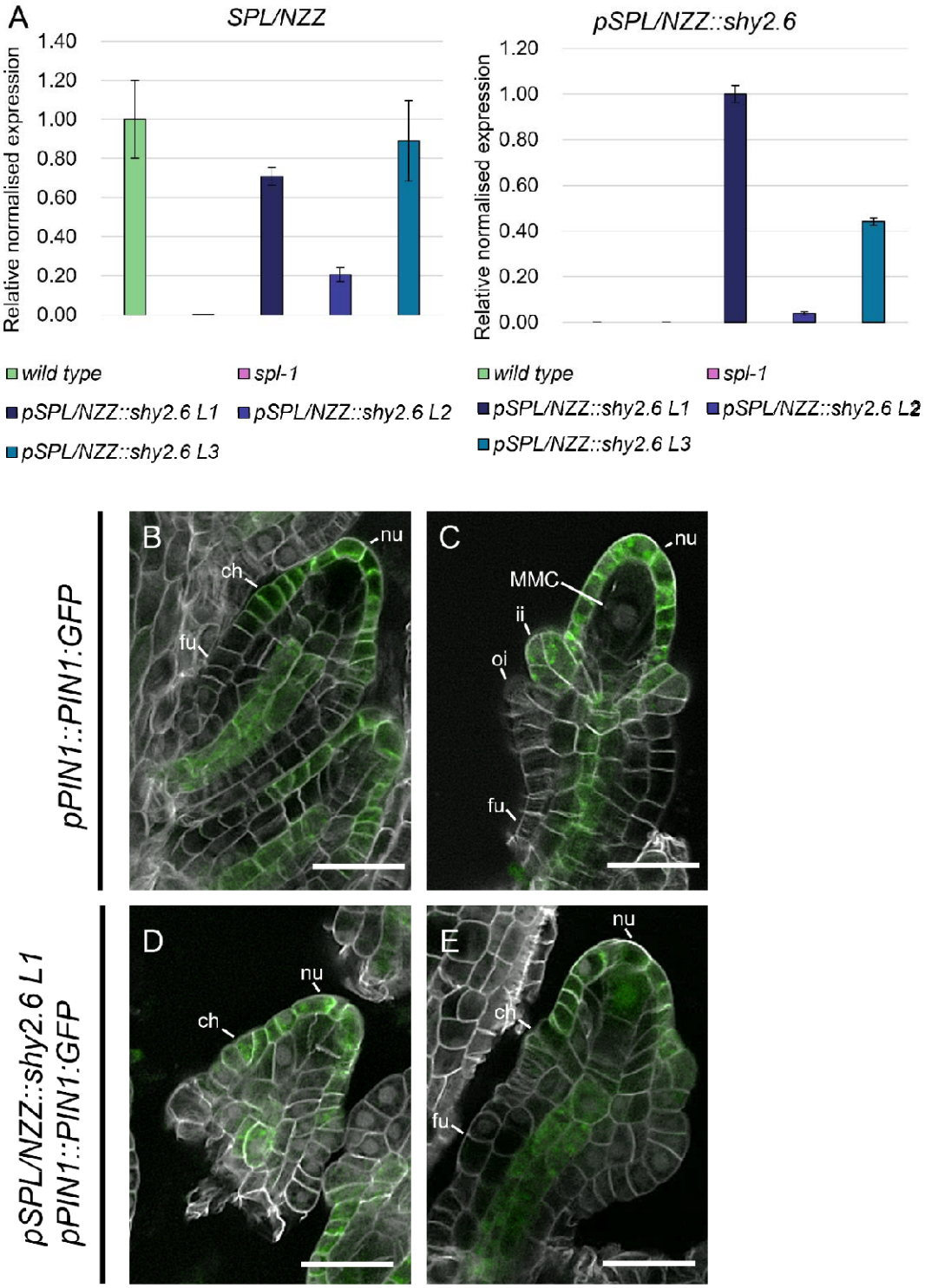

Supplementary Figure 8: *pSPL/NZZ::shy2.6* expression level and PIN1-GFP accumulation in *pSPL/NZZ::shy2.6.* (**A**) Bar plot showing *SPL/NZZ* and *pSPL/NZZ::shy2.6* relative normalised expressions in inflorescences from wild type, *spl-1* and three independent *pSPL/NZZ::shy2.6* lines. *ACTIN8* was used as housekeeping gene

for normalisation. Bars represent the mean ± SEM of the expression, as evaluated from three technical replicates per each sample. (**B**-**E**) PIN1-GFP accumulation in wild type (**B**, **C**) and *pSPL/NZZ::shy2.6 L1* (**D**, **E**) ovules at stages 2-I (**B**, **D**) and 2-III (**C**, **E**). Abbreviations: nu= nucellus; ch= chalaza; fu= funiculus; ii= inner integument; oi= outer integument; MMC= Megaspore mother cell. Scale bar = 20 µm.

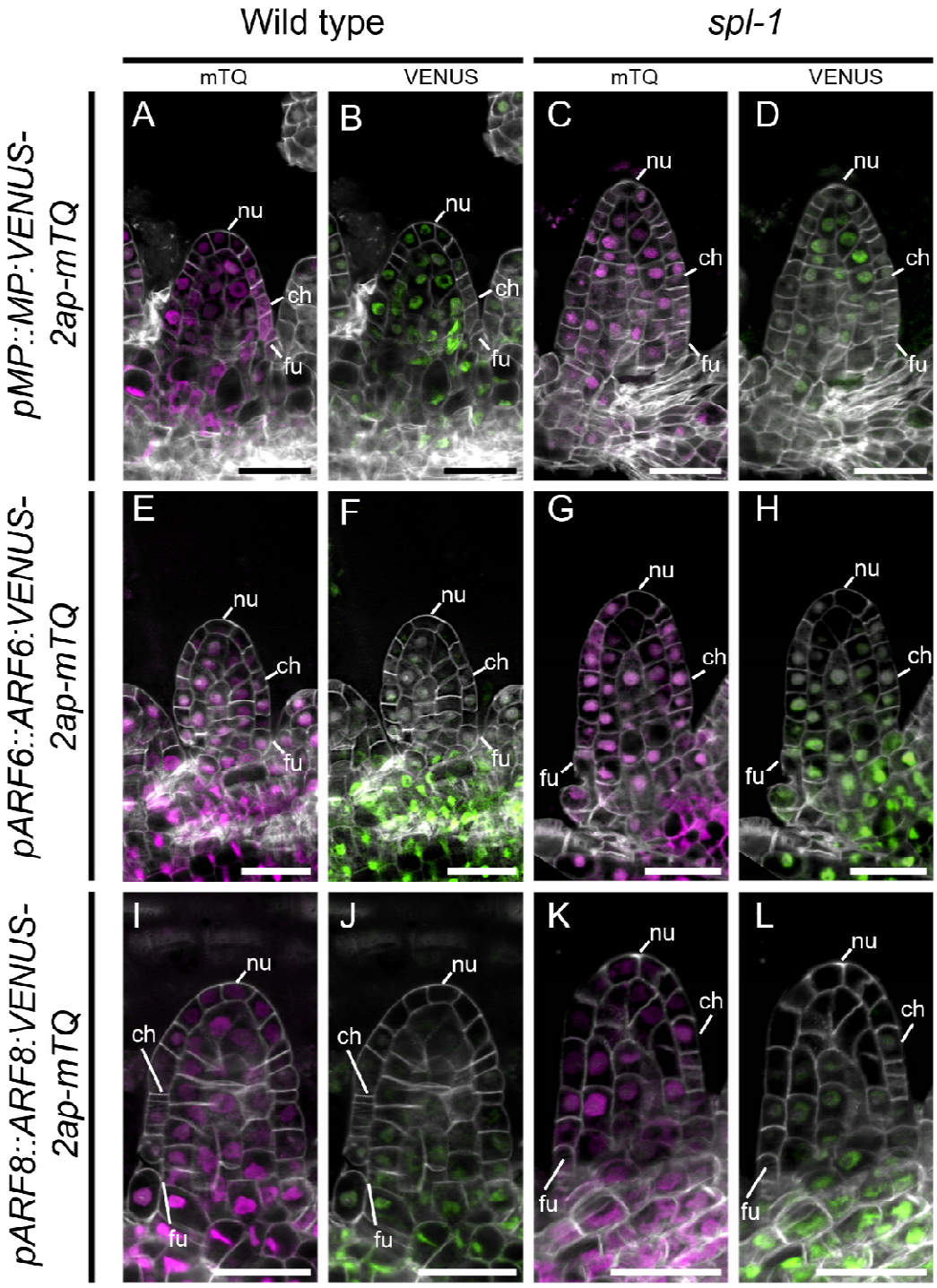

Supplementary Figure 9. ClassA ARFs expression in wild type and *spl-1* ovules. (**A-D**) *pMP::MP:VENUS-2ap-mTQ* reporter in wild type (**A**, **B**) and *spl-1* (**C**, **D**) ovules. (**E-H**) *pARF6::ARF6:VENUS-2ap-mTQ* reporter in wild type (**E**, **F**) and *spl-1* (**G**, **H**) ovules. (**I-L**) *pARF8::ARF8:VENUS-2ap-mTQ* reporter in wild type (**I**, **J**) and *spl-1* (**K**, **L**) ovules. *MP, ARF6* and *ARF8* domains of expression and translation are visualised thanks to the mTQ

signal (**A**, **C**, **E**, **G**, **I**, **K**), while domains of protein accumulation are visualised by the VENUS signal (**B**, **D**, **F**, **H**, **J**, **L**). Abbreviations: nu= nucellus; ch= chalaza; fu= funiculus. Scale bar = 20 µm.

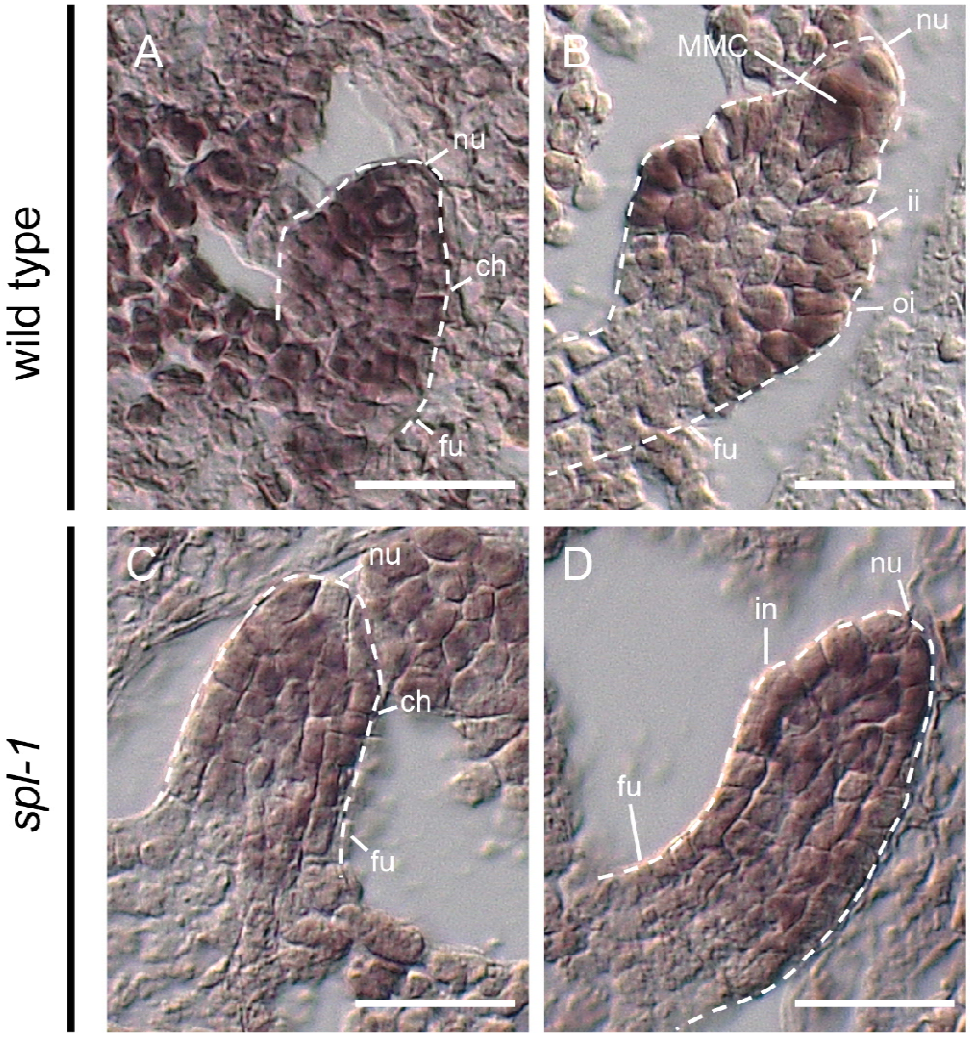

Supplementary Figure 10. ARF9 expression in wild type and *spl-1* ovules detected by *in-situ* hybridisation. (**A, D**) ISH showing *ARF9* expression in wild type ovules (**A**, **B**) and *spl-1* (**C, D**) ovules at stages 1-II (**A, C**) and 2-III (**B, D**). Abbreviations: nu= nucellus; ch= chalaza; fu= funiculus; MMC= megaspore mother cell; ii= inner integument; oi= outer integument; in= integument. Scale bar = 20 µm.

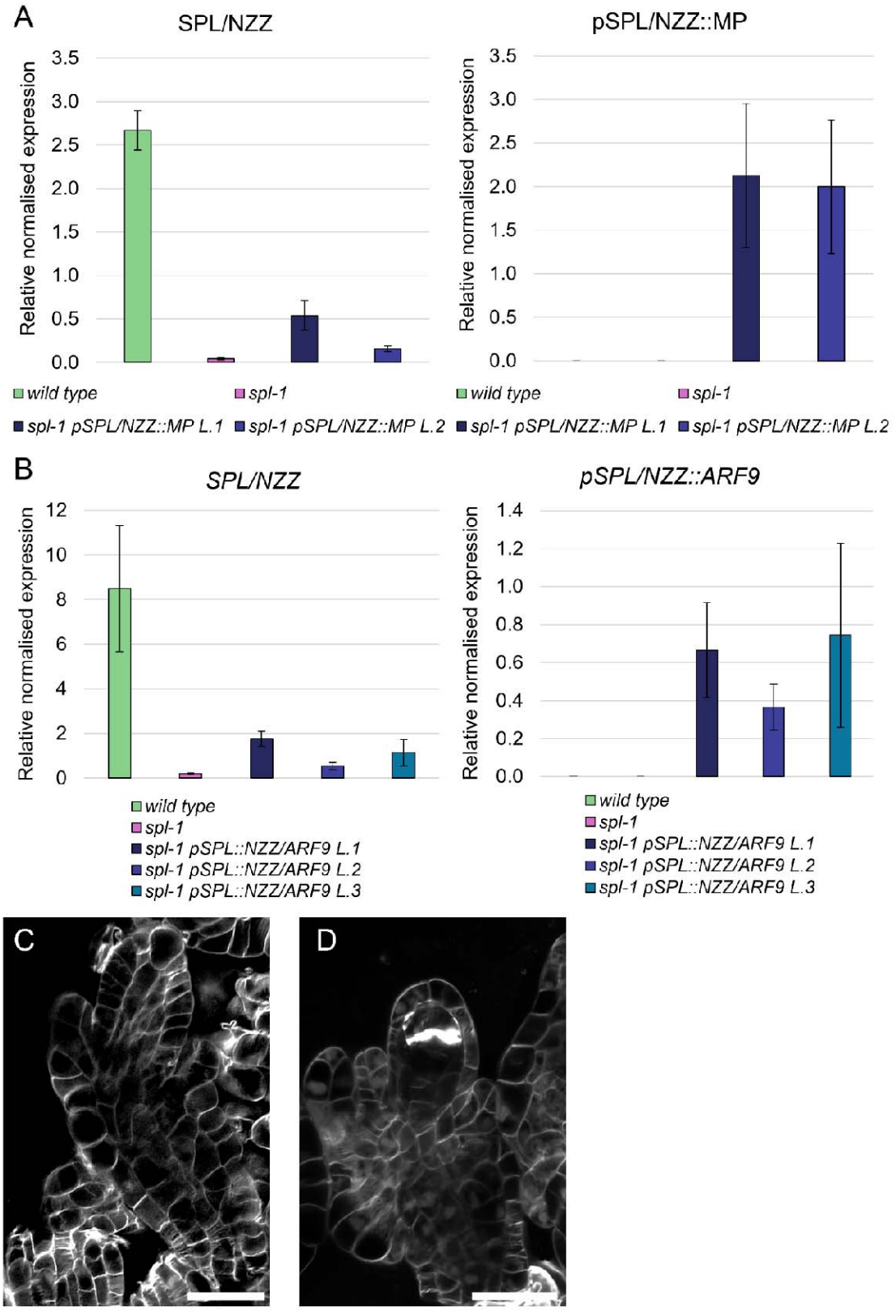
A
SPL/NZZ
pSPL/NZZ::MP
Relative normalised expression
3.5
3.0
2.5
2.0
1.5
1.0
0.5
0.0
wild type
spl-1
spl-1 pSPL/NZZ::MP L.1
spl-1 pSPL/NZZ::MP L.2
B
SPL/NZZ
pSPL/NZZ::ARF9
12
10
8
6
4
2
0
1.4
1.2
1.0
0.8
0.6
0.4
0.2
0.0
spl-1 pSPL::NZZ/ARF9 L.1
spl-1 pSPL::NZZ/ARF9 L.2
spl-1 pSPL::NZZ/ARF9 L.3
C
D

1377

1378

Supplementary Figure 11. *pSPL/NZZ::MP* and *pSPL/NZZ::ARF9* expression, *spl-1 pSPL/NZZ::MP* and *spl-1 pSPL/NZZ::ARF9* ovules at stage 2-IV. (**A**) Bar plot showing *SPL/NZZ* and *pSPL/NZZ::MP* relative normalised expressions in inflorescences from wild type, *spl-1* and two independent *spl-1 pSPL/NZZ::MP* lines. *ACTIN8* was used as housekeeping gene for normalisation. Bars represent the mean ± SEM of the expression, as evaluated from three technical replicates per each sample. (**B**) Bar plot showing *SPL/NZZ* and *pSPL/NZZ::ARF9* relative normalised expressions in inflorescences from wild type, *spl-1* and three independent *spl-1 pSPL/NZZ::ARF9* lines. *ACTIN8* was used as housekeeping gene for normalisation. Bars represent the mean ± SEM of the expression, as evaluated from three technical replicates per each sample. (**C**) In *spl-1 pSPL/NZZ::MP* ovules, the MMC does not proceed into the meiotic process. (**D**) In *spl-1 pSPL/NZZ::ARF9,* the MMC divide meiotically, as indicated by the thik callose deposition associated with the end of the meiosis I. Scale bars: 20 µm.